# Synergistic effect of mutations in the Parkinson's disease-linked proteins synaptojanin 1 and auxilin

Xin Yi Ng[1], Yumei Wu[3,5], Youneng Lin[1,5], Sidra Mohamed Yaqoob[1,5], Lois E. Greene[4], Pietro De Camilli[3], and Mian Cao[1,2]*

1. Programme in Neuroscience and Behavioural Disorders, Duke-NUS Medical School, Singapore

2. Department of Physiology, National University of Singapore, Singapore

3. Departments of Neuroscience and Cell Biology, Howard Hughes Medical Institute, Program in Cellular Neuroscience, Neurodegeneration and Repair, Kavli Institute for Neuroscience, Yale University School of Medicine, New Haven, CT 06510, USA. Aligning Science Across Parkinson's (ASAP) Collaborative Research Network, Chevy Chase, MD.

4. Laboratory of Cell Biology, NHLBI, National Institutes of Health, MD, USA

5. These authors contributed equally

* Corresponding Author
Contact Information: mian.cao@duke-nus.edu.sg

**ABBREVIATIONS:**

AADC: Aromatic l-amino acid decarboxylase
AP2: Adaptor protein complex 2
CCVs: Clathrin coated vesicles
ChAT: Choline acetyltransferase
ChINs: Cholinergic interneurons
DA: Dopamine
DAergic: Dopaminergic
DAT: Dopamine transporter
GAK: Cyclin G-associated kinase
GFAP: Glial fibrillary acidic protein
GWAS: Genome-wide association study
H&E: Hematoxylin and eosin
Iba1: Ionized calcium-binding adapter molecule 1
KI: Knock-in
KO: Knockout
LOF: Loss-of-function
MSNs: Medium spiny neurons
PD: Parkinson's Disease
SJ1: Synaptojanin 1
SN: Substantia nigra
SV: Synaptic vesicle
SV2: Synaptic vesicle glycoprotein 2
Syt1: Synaptotagmin 1
THINs: TH-positive interneurons
VTA: Ventral tegmental area

## Abstract

Parkinson's disease (PD) is a neurodegenerative disorder characterized by defective dopaminergic (DAergic) input to the striatum. Mutations in two genes encoding synaptically-enriched clathrin-uncoating factors, synaptojanin 1 (SJ1) and auxilin, result in PD. SJ1 knock-in (SJ1-KI$^{RQ}$) mice carrying PD mutation display neurological manifestation reminiscent of PD. Here we report that auxilin knockout (Aux-KO) mice display dystrophic changes of a subset of nigrostriatal DAergic terminals similar to those of SJ1-KI$^{RQ}$ mice. Furthermore, Aux-KO/SJ1-KI$^{RQ}$ double mutant mice have shorter lifespan and more severe synaptic defects than single mutant mice. These include more numerous dystrophic striatal nerve terminals positive for DAergic markers and for the PD risk protein SV2C, as well as adaptive changes in striatal interneurons. The synergistic effect of the two mutations demonstrates a special lability of DAergic neurons to defects in clathrin uncoating, with implications for PD pathogenesis in at least some forms of this condition.

**Key words**: Synaptojanin1, auxilin, clathrin, DAergic terminals, Parkinson's disease

## Introduction

Parkinson's disease (PD) is the most common neurodegenerative movement disorder characterized by selective degeneration of nigrostriatal dopaminergic (DAergic) neurons and dopamine (DA) deficiency in striatum. Genetic studies have identified more than 20 genes responsible for familial PD and 90 risk loci in sporadic PD [1,2]. These findings have implicated several cellular mechanisms in the pathogenesis of PD, including impaired protein degradation, aggregation of misfolded proteins, mitochondrial perturbations, neuroinflammation and membrane traffic dysfunction [3]. Among the latter, membrane traffic defects at synapses are believed to be an early event in PD pathogenesis, followed by axonal degeneration and loss of neuronal cell bodies in the midbrain ("dying back" mechanism) [4,5].

Two pre-synaptically enriched genes whose loss-of-function (LOF) mutations cause rare cases of familial recessive early onset PD encode auxilin (also called DNAJC6) and synaptojanin 1 (SJ1), hence defined as PARK19 and PARK20 [6-9], respectively. Interestingly, these two proteins function at different steps, but synergistically, in the shedding of the clathrin coat that follows clathrin-dependent vesicle budding to generate new synaptic vesicles (SVs) (Fig. 2a) [10]. SJ1, a phosphatase that dephosphorylates sequentially PI(4,5)$P_2$ via tandemly

145 arranged 5-phosphatase and 4-phosphatase domains, mediates the dissociation from the
146 membrane of the endocytic clathrin adaptors (the inner layer of the coat), whose membrane
147 interaction is $PI(4,5)P_2$ dependent [11]. Auxilin, a clathrin-binding co-chaperone, recruits the
148 ATPase HSC70 to dissemble the clathrin lattice, i.e. outer layer of the coat [11]. Moreover, since
149 auxilin contains a binding domain for monophosphoinositides [12], its recruitment was proposed
150 to be controlled, at least in part by the activity of SJ1.

151 Complete LOF of SJ1 results in early postnatal death [13,14], while the well characterized R258Q
152 mutation responsible for PD selectively impairs the function of its 4 phosphatase domain (also
153 called Sac domain) [7]. In the case of auxilin, most of PD mutations are complete or very strong
154 LOF mutations [15]. PD patients carrying mutations in these two genes share similar clinical
155 manifestations: recessive transmission, early or juvenile onset, typical motor deficits with
156 atypical epilepsy and developmental delay in some patients, and DA deficiency as detected
157 by reduced DaTScan signal in the striatum [15,16]. In addition, SJ1 expression level was found
158 to be reduced in postmortem PD patient brains [17,18], the connection of SJ1 with PD genome-
159 wide association study (GWAS) loci was recently reported [19], and auxilin/DNAJC6 mutations
160 were also identified in some sporadic PD patients [20], suggesting that impaired function of these
161 two proteins could play a more common role in the pathogenesis of PD and not be restricted
162 to rare familial cases.

163 Several animal models have been generated and characterized for both PD genes. Knock-in
164 (KI) mice carrying the Sac domain mutation R258Q (R259Q in mice, referred henceforth as
165 SJ1-$KI^{RQ}$ mice), recapitulated patients' neurological manifestations [21]. Nerve terminals of
166 these mice exhibited accumulation of clathrin coated vesicles (CCVs) and SV endocytosis
167 defects. Importantly, selective synaptic abnormalities were observed in nigrostriatal DAergic
168 nerve terminals of these mice, i.e. the axonal projections specifically degenerated in PD [21].
169 Perturbation of autophagosome formation was also reported in neuronal cultures of these
170 mice [22], in patient iPSC-derived human DA neuronal models carrying the same mutation and
171 in nerve terminals of *Drosophila* carrying the corresponding mutation [23]. Motor symptoms,
172 endocytic defects at synapses and degeneration of DAergic nerve terminals were also
173 reported in aged SJ1 Heterozygous (+/-) mice [18]. Moreover, a strong synthetic interaction was
174 observed in mice between the SJ1 R258Q mutation and the loss of Sac2, a PI4P phosphatase
175 shown by GWAS to be a candidate PD risk gene [24].
176
177 LOF animal models of auxilin also have features of PD pathogenesis. Reduced auxilin level
178 in *Drosophila* leads to PD-like motor symptoms and accelerates $\alpha$-synuclein mediated DA
179 neuron loss [25]. Auxilin mutant flies are also more sensitive to the environmental toxin paraquat

180 [25]. Auxilin KO mice (Aux-KO mice) are born with a lower than normal mendelian ratio and a
181 subset die perinatally [26]. The remaining ones, where the levels of the auxilin paralogue, cyclin
182 G-associated kinase (GAK) was found to be upregulated, were reported to have a normal life-
183 span, although a systematic analysis of their neurological performance was not carried out. In
184 neuronal cultures derived from these mice impaired SV endocytosis and clathrin uncoating
185 defects were observed [26]. A mouse model carrying the auxilin PD-linked mutation R927G
186 showed motor impairments in old mice, and both SV recycling and Golgi trafficking defects [27].
187 Finally, in human midbrain-like organoids, mutations of auxilin were shown to cause key PD
188 pathologic features and also neurodevelopmental defects due to impaired WNT-LMX1A
189 signaling [28].
190
191 The implication in PD of two genes that have cooperative function in clathrin uncoating during
192 SV recycling strongly suggest that their mutations result in PD via a same pathogenetic
193 mechanism. Elucidating such mechanism may offer the possibility of developing intervention
194 strategies to prevent the onset of PD manifestations in individual homozygous for these
195 mutations. It is also possible that mutations of other PD genes may converge on such
196 mechanisms, so that studies on SJ1 and auxilin may have more general implications.
197
198 Here we set out to investigate whether loss of auxilin function in mice phenocopies the
199 dystrophic changes that we have observed in the striata of SJ1-KI$^{RQ}$ mice and to determine
200 whether the combined loss of auxilin and the PD mutation of SJ1 results in synergistic effects
201 on such changes. Our results demonstrate a similar effect of the two genetic perturbations on
202 nigrostriatal DAergic nerve terminals. We also show that Aux-KO/SJ1-KI$^{RQ}$ double mutant
203 mice have a much shorter life span than single mutants and more severe dystrophic changes
204 in the striatum. Together, our results validate the use of mice that harbor these mutations as
205 model systems to study mechanisms in PD pathogenesis.
206
207 **Results**
208 **Neurological defects in Aux-KO mice that survive early postnatal death**
209 As previously reported and also shown in Fig. 2b, a subset of Aux-KO mice dies shortly after
210 birth. The survivors can have a life-span similar to wild-type (WT) controls but a subset of them
211 develop early-onset tonic clonic epileptic seizures starting at 3-4 postnatal week
212 (Supplementary Mov. 1), a finding also reported in the clinical cases carrying auxilin mutations.
213 A hindlimb clasping phenotype, a sign of neurodegeneration, was observed in some of them
214 (about 30% at 1-month) (Fig. 1a). Moreover, at 2-4 months they showed a mild fine motor
215 deficit in the balanced beam test with significantly more missteps as they walk along the beam
216 (Fig. 1b, c and Supplementary Mov. 2a, 2b), while their performance on rotarod (gross motor)

217 was normal (Fig. 1d). These results show that Aux-KO have at least some of the features
218 observed in patients carrying auxilin PD mutations.
219
220 **Defects of DAergic nerve terminals in the dorsal striatum of Aux-KO mice**
221 The previously reported analysis of cultured neurons of Aux-KO mice demonstrated
222 perturbations consistent with a defect in clathirn uncoating. To examine the impact of auxilin
223 LOF on the DAergic nigrostriatal pathway, we performed immunohistochemistry on brain
224 frozen sections using antibodies directed against tyrosine hydroxylase (TH) and the plasma
225 membrane dopamine transporter (DAT), two markers of DA neurons. Similar to SJ1-KI$^{RQ}$ mice,
226 scattered abnormal TH- and DAT-positive clusters, also positive for the plasma membrane
227 marker SNAP25 (see Supplementary Fig. 8a), were observed in the striata of these mice, but
228 not in WT and heterozygous littermates, in addition to the normal diffuse punctate
229 immunoreactivity representing axon terminal varicosities of DAergic neurons (Fig. 1e).
230 Typically, these clusters were localized next to the soma of striatal neurons. Electron
231 microscopy (EM) observations of SJ1-KI$^{RQ}$ striata had shown that the presence of these
232 TH/DAT positive clusters correlated with the occurrence of abnormal nerve terminals
233 characterized by peculiar onion-like plasma membrane accumulations. Accordingly, similar
234 structures were detected by EM in auxilin KO striata (see Fig. 5). Interestingly, as in the case
235 of SJ1-KI$^{RQ}$ brains, these clusters were specifically present in the dorsal but not ventral
236 striatum (Fig. 1e). Thus, nerve terminals of the nigrostriatal DA system are selectively and
237 similarly affected by either complete LOF of auxilin or the R258Q mutation in SJ1, two genetic
238 perturbations that result in PD in human patients. Tiny DAT-positive clusters first appeared at
239 about 3-week and large clusters positive for both DAT and TH peaked at 1-2 months. However,
240 in both adult (5-month) and aged mice (12-month), the size and number of these clusters were
241 significantly reduced (Fig. 1f, g), similar to what we observed in SJ1-KI$^{RQ}$ mice (Fig. 1h, i).
242 Possibly, structural changes of a subset of DAergic nerve terminals only occurs at a young
243 age and these terminals eventually degenerate. However, the occurrence of a repair
244 mechanism cannot be excluded.
245
246 **More severe neurological phenotypes in Aux-KO/SJ1-KI$^{RQ}$ double mutant mice than in**
247 **single mutant mice**
248 The similar clinical phenotypes of PD mutations in SJ1 (RQ mutation) and auxilin (complete
249 LOF) and the similar cellular and histological phenotypes observed in SJ1-KI$^{RQ}$ and Aux-KO
250 mice prompted us to examine a synergistic effect of the two genetic disruptions by generating
251 Aux-KO/SJ1-KI$^{RQ}$ double mutant mice. As shown in Fig. 2b, Aux-KO/SJ1-KI$^{RQ}$ mice have
252 much shorter lifespan compared to either single mutant mice, revealing a strong synthetic
253 genetic interaction. About 75% of Aux-KO/SJ1-KI$^{RQ}$ mice died within 1 month after birth.

254 Moreover, they were usually smaller in size (Supplementary Fig. 1a, b) and showed hindlimb
255 clasping and seizures. To date, only one Aux-KO/SJ1-KI$^{RQ}$ mouse out of more than 50
256 survived to adulthood and died suddenly at 7-month-old. As assessed by the balanced beam
257 test and by immunohistological analysis, this mouse had more severe motor coordination
258 defect and DAergic terminal dystrophy compared to single mutant mice (Supplementary Mov.
259 3a-d and Supplementary Fig. 10).
260
261 Hematoxylin and eosin (H&E) staining of Aux-KO/SJ1-KI$^{RQ}$ mouse brains at 1-month of age
262 (the age at which nearly 50% of the double mutant mice survived) revealed a normal brain
263 architecture (Supplementary Fig. 1c). Likewise, no obvious gliosis was observed in different
264 brain regions, upon immunostaining with ionized calcium-binding adapter molecule (Iba1), a
265 microglia marker and glial fibrillary acidic protein (GFAP), an astrocyte marker (Supplementary
266 Fig. 2). Moreover, western blot analysis of total homogenates of brains at the same age
267 showed that, at least at this age, the levels of major synaptic proteins tested, including SV
268 proteins, endocytic proteins and proteins of DA metabolism were unchanged, with the
269 exception of a modest upregulation of amphiphysin 2 and endophilin1 in SJ1-KI$^{RQ}$
270 (Supplementary Fig. 3a, b).
271
272 **Synergistic disrupting effects of auxilin and SJ1 mutations on clathrin coat dynamics**
273 **in nerve terminals**
274 Synapses of either Aux-KO or SJ1-KI$^{RQ}$ mice display abnormal presynaptic clustering of
275 endocytic factors, as revealed by immunofluorescence (Fig. 2), and an accumulation of CCVs,
276 and also of empty clathrin cages in the case of Aux-KO neurons, as revealed by EM (Fig. 3).
277 These defects, which result in defective endocytic recycling of SVs, are not restricted to
278 DAergic nerve terminals in agreement with the ubiquitous expression of SJ1 and auxilin in
279 neurons. Moreover, they are generally more prominent at inhibitory nerve terminals as labeled
280 by GAD65, which have higher tonic levels of activity (Fig. 2e). Both these defects were more
281 severe at synapses of double mutant neurons. At these synapses, the fluorescence intensity
282 of clusters of endocytic proteins, such as clathrin, adaptor protein 2 (AP2), SJ1, amphiphysin
283 1 and amphiphysin 2, which was already higher in Aux-KO and SJ1-KI$^{RQ}$ single mutant
284 neurons than in WT, was even higher in Aux-KO/SJ1-KI$^{RQ}$ neurons (Fig. 2c, d).
285
286 A synergistic effect of the two mutations could also be observed by EM, as shown by
287 representative EM micrographs in Fig. 3a, and by a morphometric analysis of CCVs and empty
288 clathrin cages in nerve terminals of the striatum (Fig. 3b). As expected, the SJ1-KI$^{RQ}$ mutation
289 resulted primarily in an increase in CCVs and the Aux-KO mutation also resulted in an increase
290 of empty clathrin cages, but the combination of the two mutations led to an overall increase in

291 assembled clathrin (both cages or coated vesicles). At some inhibitory synapses in other
292 regions of the brain such increase was huge, as illustrated by the three examples of inhibitory
293 nerve terminals in the deep cerebellar nuclei shown in Fig. 3c that show massive
294 accumulations of empty clathrin cages and CCVs.
295
296 **Enhanced dystrophic changes in the striatum of Aux-KO/SJ1-KI$^{RQ}$ double mutant mice**
297 We next focused on the DA system in both midbrain and striatum. The morphology of TH
298 positive DA neurons in both substantia nigra (SN) and ventral tegmental area (VTA) looks
299 normal in 1-month-old Aux-KO/SJ1-KI$^{RQ}$ mice compared to WT controls (Supplementary Fig.
300 4a). However, in the striatum of Aux-KO/SJ1-KI$^{RQ}$ mice, the DAergic nerve terminal dystrophic
301 phenotype was more severe than in the single mutant mice. The number of TH/DAT-positive
302 clusters, also positive for SNAP25 (see Supplementary Fig. 8a) was significantly increased
303 compared to single mutants, although the size of clusters was not changed (Fig. 4a, b). More
304 importantly, similar TH/DAT-positive clusters were also observed in the ventral striatum
305 (including both the nucleus accumbens and olfactory tubercle) of Aux-KO/SJ1-KI$^{RQ}$ mice, but
306 not of the single mutant mice (Fig. 4c, d and Supplementary Fig. 4b, 5). Since the ventral
307 striatum receives DAergic axonal input from the VTA of the midbrain, this result indicates that
308 the combined perturbation of auxilin and SJ1 affects more globally the function of DAergic
309 neurons of the midbrain. It suggests a vulnerability of both SN and VTA DAergic neurons to
310 the combined loss of SJ1 and auxilin, but a lower tolerance of SN neurons to the loss of either
311 one of these two proteins.
312
313 EM observations confirmed that the increase of TH/DAT-positive clusters corresponded to an
314 increase in the number of onion-like plasma membrane derived structures resulting in multiple
315 cytoplasmic lamellae. While these structures were difficult to be found in thin sections of single
316 mutant mice due to their scattered distribution, they were much easier to be found in thin
317 section of double mutant striata, confirming their abundance (Fig. 5). Red arrowheads in Fig.
318 5 show that they represent plasma membrane invagination. Lamellae often contained
319 scattered small SV clusters or CCVs consistent with their axonal nature. Moreover, anti-TH
320 immunogold labeling confirmed that these structures corresponded to TH accumulations
321 (Supplementary Fig. 6).
322
323 Immunofluorescence for a variety of nerve terminal proteins and specific components of the
324 DAergic system revealed co-enrichment of several other proteins with TH and DAT in these
325 structures in Aux-KO/SJ1-KI$^{RQ}$ mice. These included aromatic L-amino acid decarboxylase
326 (AADC), the enzyme that acts downstream of TH to convert levedopa into DA and thus is
327 another marker of DAergic neurons (Fig. 6a), the plasma membrane marker SNAP25 (Fig. 6b)

328 and a subset of SV proteins, such as synaptic vesicle glycoprotein 2C (SV2C) (Fig. 6c) and
329 synaptotagmin 1 (Syt1) (Supplementary Fig. 7c) but not other SV house-keeping proteins such
330 as SV2B (Fig. 6d) and synapsin (Supplementary Fig. 7d). Both AADC and SV2C also cluster
331 with TH/DAT in Aux-KO or SJ1-KI$^{RQ}$ striatum (Supplementary Fig. 7a, b). Given the very low
332 numbers of SVs in the onion-like structures but the abundance of plasma membrane, SV2C
333 and Syt1 may be more prone than others to become stranded in the plasma membrane in
334 double mutant neurons. SV2C immunoreactivity was particularly strong consistent with a
335 preferential expression of this SV2 isoform in the striatum and the midbrain, relative to SV2A
336 and SV2B (http://dropviz.org/ and [29,30]). Interestingly, SV2C was recently identified as a PD
337 risk gene [31,32]. Importantly, the abnormal SNAP25 positive clusters were not observed in other
338 brain regions, suggesting a selective impairment in the striatum (Supplementary Fig. 8b).
339 None of the endocytic proteins tested, including clathrin light chain (CLC) and endophilin 1
340 were found in these aggregates (Fig. 6e, f), in agreement with the absence of accumulation
341 of endocytic intermediates observed by EM at these sites.
342
343 **Adaptive upregulation of striatal TH/AADC positive interneuron and SV2C positive**
344 **cholinergic interneurons in Aux-KO/SJ1-KI$^{RQ}$ mice.**
345 Most interestingly, we also detected some protein expression changes in local striatal neurons
346 of Aux-KO/SJ1-KI$^{RQ}$ mice. First, in sections of mutant striata immunolabeled with anti-TH
347 antibody, in addition to the presence of TH-positive normal and abnormal nerve terminals
348 which co-localized with DAT immunoreactivity, we also observed sparsely distributed TH-
349 positive interneuron (THIN) cell bodies, different from Darpp32-positive medium spiny neurons
350 (MSNs) which account for the predominant population in the striatum (Supplementary Fig. 9a).
351 These neurons were not visible in WT and Aux-KO striata, and were only occasionally
352 observed in SJ1-KI$^{RQ}$ (Fig. 7a, b). Such neurons were also positive for AADC (Fig. 7c),
353 suggesting that they can generate DA, although they were positive for GABA as well
354 (Supplementary Fig. 9b), and negative for DAT (Fig. 7a). Second, we detected another
355 neuronal population which was strongly labeled with two different SV2C antibodies in Aux-
356 KO/SJ1-KI$^{RQ}$ striata (Fig. 7d and Supplementary Fig. 9c, d). These SV2C-positive neuronal
357 cell bodies did not overlap with TH/AADC-positive neurons, but were all positive for choline
358 acetyltransferase (ChAT), a marker of striatal cholinergic interneurons (CHINs) (Fig. 7e and
359 Supplementary Fig. 9c, d). Compared to WT sections where the SVC2 signal was low, SV2C
360 expression was much higher in a subset of ChAT-positive neurons in Aux-KO/SJ1-KI$^{RQ}$ (Fig.
361 7f, g and Supplementary Fig. 9e, f). The intensity, number and distribution of ChAT remains
362 unchanged between WT and Aux-KO/SJ1-KI$^{RQ}$ (Fig. 7f, g), suggesting this is a specific
363 upregulation of SV2C in the ChINs. We further examined other cell types in the striatum using
364 immunofluorescence against Darpp32 for MSNs, against GFAP for astrocytes and against

365 Iba1 for microglia. Both MSNs and glia cells appeared normal in morphology, localization and
366 fluorescence intensity (Supplementary Fig. 7e, f, g). These findings suggest that the local
367 striatal microcircuitry has been affected in Aux-KO/SJ1-KI$^{RQ}$ mutant mice. Whether this is a
368 secondary effect to compensate for DA deficiency from DAergic terminals, or a cell
369 autonomous effect resulting from the absence of SJ1/auxilin in these interneurons requires
370 further investigation.
371
372 **Discussion**
373 In this study we show that LOF mutations in two PD-linked proteins implicated in endocytic
374 clathrin-mediated budding at synapses, SJ1 and auxilin, produce similar dystrophic changes
375 of nigrostriatal DAergic nerve terminals. Moreover, we show a strong synthetic interaction of
376 SJ1 PD mutation and auxilin KO. These findings provide striking evidence for the proposed
377 functional partnership of the two proteins in clathrin coat shedding, with the phosphoinostide
378 phosphatase activity of SJ1 being responsible for the dissociation of the clathrin adaptors from
379 the membrane and auxilin playing a critical role, along with the chaperone HSC70, in the
380 disassembly of the clathrin coat. In fact, the phosphoinositide phosphatase activity of SJ1 was
381 proposed to help recruit auxilin. Importantly, they point to dysfunction in clathrin uncoating as
382 one of the perturbations that can lead to early onset PD. How such dysfunction in turn leads
383 to disease remain to be further clarified. Mechanisms may include a defect in SV recycling
384 with an impact of DA release, other alterations of synaptic membrane traffic such as
385 impairment of autophagosome formation, sequestration of critical factors by assembled
386 clathrin. As SJ1 and auxilin are neuronal housekeeping proteins, a major open question is
387 why the DAergic system more severely affected, although, as previously shown by us and
388 others, synaptic defects in SJ1-KI$^{RQ}$ and in auxilin mutant mice are not restricted to DAergic
389 neurons.
390
391 Aux-KO mice have phenotypic manifestations that resemble those of SJ1-KI$^{RQ}$ mice, and both
392 of them recapitulate some of the manifestations of human PD patients carrying mutations in
393 the auxilin/PARK19 and the synaptojanin1/PARK20 genes. However, the neurological defects
394 of Aux-KO mice are less severe than those of SJ1-KI$^{RQ}$ mice. This is probably due to the
395 presence and compensatory upregulation of the auxilin paralogue auxilin-2/GAK in Aux-KO
396 mouse brains [26]. GAK itself was identified as a PD risk gene via a GWAS study [33].
397
398 Both the SJ1-KI$^{RQ}$ mouse model and the auxilin KO model have been reported to show
399 presynaptic clustering of endocytic factors and accumulations of assembled clathrin [21,26].
400 These clathrin structures were different in the two genotypes: primarily CCVs in SJ1-KI$^{RQ}$ mice
401 while empty clathrin cages in Aux-KO mice, as in the absence of auxilin spontaneously

402 assembled cytosolic clathrin does not disassemble. These changes were widespread across
403 the brain, but more prominent at inhibitory synapses, probably due to the tonic firing pattern
404 in these synapses which requires more efficient SV recycling, making these synapses more
405 vulnerable to endocytic defects. A similar difference in the impact of endocytic protein
406 mutations on excitatory and inhibitory synapses was also observed in SJ1 KO [34] and dynamin
407 KO mice [35]. The imbalanced excitatory/inhibitory synaptic transmission in SJ1-KI$^{RQ}$ mice and
408 Aux-KO mice could explain the epileptic seizures observed in both human patients and mice
409 with mutations in SJ1 and auxilin.
410
411 The most interesting new observation that we have made in Aux-KO mice is the occurrence
412 of histological defects in their striatum which are similar to those that we had observed in the
413 striatum of SJ1-KI$^{RQ}$ mice [21]. These consist of TH/DAT positive structures that reflect presence
414 of dystrophic DAergic nerve terminals and correlate with abnormal onion-like plasma
415 membrane infoldings detectable by EM. The occurrence of these histological/cellular
416 phenotypes in both mutant mouse models is a striking PD-relevant finding as it suggests a
417 special lability of nigrostriatal DA neurons to perturbation of endocytic clathrin coat dynamics.
418
419 As we discussed in our study of SJ1-KI$^{RQ}$ mice, these onion-like structures appear to originate
420 primarily by invaginations of the plasma membrane, as shown by EM and by their enrichment
421 in two plasma membrane proteins DAT and SNAP25. Possibly, they are resultant of endocytic
422 failure at a subset of synapses. However, they are not enriched in endocytic proteins and in
423 several house-keeping SV proteins, consistent with the lack of enrichment of SVs in these
424 terminals, although they are enriched in SV2C, raising the possibility that this SV protein may
425 remain stranded in the plasma membrane. Interestingly, SV2C, which is the SV2 family
426 member expressed in DAergic neurons and is a modulator of DA release [29], was recently
427 identified by GWAS from both Asian and European cohorts as a PD candidate risk gene [31,32].
428 Moreover, in both mutant genotypes, presence of these structures peak at 1-2 months but
429 they decrease as mice get older (5 and 12 months), revealing either repair mechanisms or
430 removal of degenerated nerve terminals in older mice. Interestingly, a follow up study on PD
431 patients carrying the SJ1 RQ mutation showed relatively stability of clinical manifestations at
432 later stages [36]. The early onset feature in both models also suggests there may be some
433 neurodevelopmental defects due to LOF of SJ1 or auxilin. Indeed, PD patients carrying both
434 genes' mutations suffer from developmental delay [15,16], and a recent study of human midbrain-
435 like organoids carrying the auxilin PD mutation also showed impaired WNT-LMX1A signal
436 during DA neuron development [28].
437

438 The strong synthetic effect of the SJ1-KI$^{RQ}$ mutation and the Aux-KO mutation is a key result
439 that provides evidence for a similar PD pathogenetic mechanism resulting from mutations in
440 these two proteins. Relative to single mutants, double mutant mice have much shorter lifespan
441 and usually die between 3 to 4 weeks after birth, which is the critical period for
442 neurodevelopment in rodents [37]. Moreover, they display enhanced clustering of endocytic
443 proteins and more abundant dystrophic TH/DAT/AADC and SV2C positive nerve terminals,
444 which additionally are not restricted to the dorsal striatum as in single mutant mice, but are
445 also present in the ventral striatum. Thus, there appears to be a different threshold of DAergic
446 neurons to the combined SJ1 and auxilin perturbation in the SN and VTA that project to the
447 dorsal and ventral striatum, respectively. One factor that may contribute to the vulnerability of
448 DAergic neuron to disruptions of two endocytic proteins may be their tonic firing activity, which
449 may require efficient SV recycling to sustain continuous release of DA. But this is not a unique
450 property of these neurons.
451
452 A striking finding in Aux-KO/SJ1-KI$^{RQ}$ striata, besides the presence of dystrophic DAergic
453 nerve terminals, was the presence of changes in two different types of interneurons, which
454 likely reflect adaptive modifications. First, there was an increase in the number of TH positive
455 THINs. THINs were also positive for AADC, suggesting they can potentially synthesize DA. A
456 similar increase was previously reported in neurotoxin-induced rodent and non-human primate
457 PD models [38,39], as well as in a genetic PD mouse model [40], and was interpreted as a
458 compensatory change due to loss of DAergic terminals. The increase that we have observed
459 in Aux-KO/SJ1-KI$^{RQ}$ striata may have a similar explanation. However, DAT is not detected in
460 these TH/AADC positive interneurons, suggesting they are not “authentic” DA neurons [41].
461 Second, in addition to the accumulation of SV2C with TH and DAT in DAergic terminals, we
462 also observed upregulated SV2C expression in the soma of another subset of striatal
463 interneurons, the ChAT positive giant ChINs. Expression of SV2C in striatal ChINs has
464 previously been reported [42,43], but such expression is robustly increased in Aux-KO/SJ1-KI$^{RQ}$
465 striata, while expression of ChAT remains unchanged. Interestingly, a study using neurotoxin
466 PD mouse models to deplete DA also showed a significant increase in striatal SV2C mRNA
467 levels [44]. Considering that an imbalance of DAergic and cholinergic signals in the striatum is
468 a feature of PD [45] and that SV2C has been linked by multiple studies to PD [29,31,32,44,46], this
469 adaptive change in Aux-KO/SJ1-KI$^{RQ}$ striata deserves further investigation.
470
471 In conclusion, we have reported here strong evidence for the hypothesis that mutations in SJ1
472 and auxilin may lead to PD via a similar pathogenetic mechanism. Several PD causative genes
473 have now been identified. The next goal is to identify cellular process onto which the function
474 of these genes converges, as such identification will provide insight into pathogenetic

475 mechanisms with implication for therapeutic approaches. After the well-established
476 partnership of PINK1 and Parkin, the cooperation of SJ1 and auxilin is the second clear
477 example of functional partnership between two PD genes. Interestingly, we previously
478 reported a synergistic function of SJ1 with another phosphoinositide phosphatase, Sac2,
479 which GWAS studies had indicated as a candidate PD risk gene. Thus, we anticipate that
480 further studies of auxilin and SJ1 will provide valuable insight into mechanisms that are at the
481 core of at least some form of PD.
482
483
484
485 **Figure Legends**
486
487 **Figure 1. Aux-KO mice exhibit parkinsonism-like phenotypes with dystrophic changes**
488 **in the DAergic axon terminals in the dorsal striatum.**
489 (a) Hindlimb clasping phenotype of 4-month-old Aux-KO mouse.
490 (b) 2-month-old Aux-KO mice have missteps while walking on the balance beam.
491 (c) Quantification for the number of missteps during the balance beam test for three different
492 age groups of Aux-KO mice. Aux-KO mice exhibit mild fine motor deficits at 2-4 months
493 compared to the Ctrl group. Above 5 months, Aux-KO mice performed similarly as Ctrl (5-8M:
494 $p$=0.8202; >9M: $p$=0.6426). Data are represented as mean ± SEM (** $p$<0.01, by Student's t
495 test). For the 2-4M group, N number is 15 and 14 for Ctrl and Aux-KO respectively. For the 5-
496 8M group, N=7 for Ctrl and N=8 for Aux-KO. Finally, N number of the >9M group is 8 and 13
497 for Ctrl and Aux-KO respectively.
498 (d) Performance of three different age groups of Aux-KO mice on the accelerated rotarod.
499 Aux-KO mice performance is similar to the Ctrl for all three age groups (2-4M: $p$=0.754; 5-8M:
500 $p$=0.115 and >9M: $p$=0.549). Data are represented as mean ± SEM. Given below are the N
501 numbers used for each age group of the Ctrl (2-4M: 15, 5-8M: 9 and >9M: 11) and Aux-KO
502 (2-4M: 13, 5-8M: 11 and >9M: 15) mice.
503 (e) Double staining for TH (green) and DAT (red) of 1-month-old Ctrl and Aux-KO mice shows
504 selective clustering of these two DAergic markers only in the dorsal but not ventral striatum.
505 (f and h) Age-dependent decrease of the number of TH/DAT positive clusters in the dorsal
506 striatum of Aux-KO and SJ1-KI$^{RQ}$ mice is observed respectively at both 5-month and 12-month.
507 (g and i) Quantification for TH and DAT clusters shown in (f) and (h). The number of clusters
508 is counted in 300 x 300-μm regions of interest (ROIs). For each mouse, five ROIs were
509 selected at random for quantification. 3 individual mice were used for each age group and
510 genotype. Data are represented as mean ± SEM (** $p$<0.01, and *** $p$<0.001, and ****
511 $p$<0.0001 by two-way ANOVA with post-hoc Tukey's test).

512

513 **Figure 2. LOF of both Auxilin and SJ1 in clathrin-mediated SV recycling exacerbate**
514 **neurological defects in Aux-KO/SJ1-KI$^{RQ}$ mice.**

515 (a) Schematic diagram displaying the role of Auxilin (PARK19) and SJ1 (PARK20) in clathrin-
516 mediated SV recycling.

517 (b) Survival curves of wild-type (WT), Aux-KO, SJ1-KI$^{RQ}$, and Aux-KO/ SJ1-KI$^{RQ}$ mice.

518 (c) Representative images of immunoreactivity for CLC, AP2, SJ1, Amphiphysin 2 and
519 Amphiphysin 1 in DIV19 cultured primary cortical neurons from Ctrl, Aux-KO, SJ1-KI$^{RQ}$ and
520 Aux-KO/ SJ1-KI$^{RQ}$ newborn pups.

521 (d) Quantification of synaptic clusters intensity shown in (c). Data are represented as mean ±
522 SEM (***p<0.001; ****p<0.0001 by one-way ANOVA with post-hoc Tukey's test). The number
523 of neurons quantified for each endocytic marker is as follow: Ctrl: n=43-49, Aux-KO: n=32-52,
524 SJ1-KI$^{RQ}$: n=35-37, Aux-KO/ SJ1-KI$^{RQ}$: n=39-44 from 4-6 independent experiments.

525 (e) Immunostaining of amphiphysin 1 with Gad65 (inhibitory presynaptic marker) in DIV19
526 cortical neurons revealed that these synaptic clustering of endocytic proteins occur
527 predominantly in GABAergic neurons.

528

529 **Figure 3. Accumulation of CCVs and empty clathrin cages in nerve terminals of Aux-**
530 **KO, SJ1-KI$^{RQ}$, and Aux-KO/ SJ1-KI$^{RQ}$ mice.**

531 (a) Representative EM micrographs of nerve terminals from the dorsal striatum of single and
532 double mutant mice. Red and black arrows point to CCVs and empty clathrin coated cages
533 (EC) respectively. Scale bar: 250 nm.

534 (b) Morphometry analysis of the number of SVs, CCVs, and ECs per pre-synaptic area in the
535 dorsal striatum (Ctrl n=124, Aux-KO n=156, SJ1-KI$^{RQ}$ n=198, and Aux-KO/ SJ1-KI$^{RQ}$ n=120).
536 Each dot represents one nerve terminal. Data are represented as mean ± SD. *$p$<0.05;
537 **$p$<0.01; ****$p$<0.0001 (One-way ANOVA with Games-Howell's multiple comparison test).

538 (c) Examples of Purkinje nerve terminals in the deep cerebellar nuclei of Aux-KO/ SJ1-KI$^{RQ}$
539 mouse showing the striking accumulation of assembled clathrin (both ECs and CCVs). The
540 tight packaging of SVs (middle and right images) was previously reported in nerve terminals
541 of SJ1-KI$^{RQ}$ mice (Cao et al. Fig. S3D) and may reflect dystrophic changes, Scale bar: 500
542 nm.

543

544 **Figure 4. DAergic axon terminals undergo dystrophic changes in both dorsal and**
545 **ventral striatum of Aux-KO/ SJ1-KI$^{RQ}$ mice.**

546 (a and c) Representative images for TH and DAT in cryopreserved-sections for 4 genotypes
547 in (a) dorsal striatum and (c) nucleus accumbens (NAc) which is part of the ventral striatum.

548

549 (b and d) Quantification for the size and average number of DAT and TH clusters in (b) dorsal
550 striatum and (d) ventral striatum. The number of clusters is calculated in five regions of interest
551 (ROIs) which were selected at random for quantification of each mouse. Data are represented
552 as mean ± SEM (***p<0.001; ****p<0.0001 by two-way ANOVA with post-hoc Tukey's test).
553 Ctrl: n=3, Aux-KO: n=4, SJ1-KI$^{RQ}$: n=3, and Aux-KO/SJ1-KI$^{RQ}$: n=4.
554
555 **Figure 5. EM micrographs showing multilayered onion-like membrane structures in the**
556 **dorsal striatum of Aux-KO, SJ1-KI$^{RQ}$, and Aux-KO/ SJ1-KI$^{RQ}$ mice.**
557 These structures, which are positive for TH immunoreactivity (see Supplementary Fig 6),
558 appear to result from invaginations of the plasma membrane as indicated by red arrowheads.
559 Note in the bottom right field presence of a cluster of SVs (black arrowheads) and scattered
560 CCVs (red arrows) and empty clathrin cages (black arrows), confirming that these structures
561 represent dystrophic changes of nerve terminals. Scale bar: 500 nm.
562
563 **Figure 6. Accumulation of other proteins with TH/DAT in dystrophic DAergic nerve**
564 **terminals in Aux-KO/ SJ1-KI$^{RQ}$ mice.**
565 (a) Double staining of DAT with AADC, a DA catabolism enzyme showed colocalization in
566 the striatum of Aux-KO/SJ1-KI$^{RQ}$ mice.
567 (b) Double staining of DAT with SNAP25, a plasma membrane SNARE protein showed
568 colocalization in the striatum of Aux-KO/SJ1-KI$^{RQ}$ mice.
569 (c-d) Double staining of SV2C (c) and SV2B (d) reveals that SV2C is specifically accumulated
570 in TH/DAT positive clusters in the striatum of Aux-KO/SJ1-KI$^{RQ}$ mice, but not its family
571 membrane SV2B.
572 (e-f) Double staining of clathrin light chain (e) and endophilin (f) reveals that both endocytic
573 proteins do not colocalize with TH/DAT positive clusters in the striatum of Aux-KO/SJ1-KI$^{RQ}$
574 mice.
575
576 **Figure 7. Adaptive changes of TH positive interneurons and SV2C positive cholinergic**
577 **interneurons in Aux-KO/SJ1-KI$^{RQ}$ striatum**
578 (a) Immunostaining of TH (green) and DAT (red) reveals presence of TH-positive/DAT-
579 negative neurons in the 1-month-old Aux-KO/SJ1-KI$^{RQ}$ striatum.
580 (b) Quantification for the total number of THINs in the striatum. Data are represented as mean
581 ± SEM (** $p$<0.01 by one-way ANOVA with post-hoc Tukey's test). Ctrl: n=3, Aux-KO: n=4,
582 SJ1-KI$^{RQ}$: n=3, and Aux-KO/SJ1-KI$^{RQ}$: n=4.
583 (c) THINs also show immunoreactivity towards anti-AADC antibody.

584 (d) Representative images of SV2C and TH staining in the dorsal striatum of 1-month-old Aux-
585 KO/SJ1-KI$^{RQ}$ mice. TH and SV2C were observed to be expressed in separate neuron
586 populations. SV2C-positive/TH-negative neurons are marked by white arrows.
587 (e) Double staining of striatal region with cholinergic marker ChAT and SV2C shows overlap
588 between the two in a specific neuron subset, indicating that the SV2C positive neurons are
589 giant striatal ChINs.
590 (f) Whole-striatum imaging reveals a subset of ChAT-positive ChINs that exhibit striking
591 upregulation of SV2C in Aux-KO/SJ1-KI$^{RQ}$ mice compared to control.
592 (g) Quantification for percentage of ChAT-positive interneurons with increased SV2C
593 expression, as well as individual intensity of SV2C and ChAT in striatal ChINs. For each
594 individual mouse, 20 ChINs across the striatum were randomly selected for quantification.
595 Data is represented as mean ± SEM (* $p<0.05$ and ** $p<0.01$, by Student's unpaired t test).
596 Ctrl: n=3 and Aux-KO/SJ1-KI$^{RQ}$: n=3.
597
598 **Methods and Materials**
599 **Animals**
600 Both the Aux-KO and SJ1-KI$^{RQ}$ mice were generated as described before [21,26]. These two
601 mouse models were crossed with each other to generate the Aux-KO/ SJ1-KI$^{RQ}$ double-mutant
602 mice. Mice were housed in SPF rooms with a 12-hour light/dark cycle. All experiments
603 involving animals were conducted according to the protocol approved by SingHealth
604 Institutional Animal Care and Use Committee (IACUC).
605
606 **Antibodies**
607 The following primary antibodies were obtained from Dr Pietro De Camilli's lab at Yale
608 University: rabbit anti-SJ1, rabbit anti-Auxilin, mouse anti-Amphiphysin 1, mouse anti-Clathrin
609 Heavy Chain, rabbit anti-pan-Dynamin, rabbit anti-pan-Endophilin, mouse anti-GAD65, rabbit
610 anti-SNAP25, rabbit anti-Synapsin, mouse anti-VAMP2, rabbit anti-Synaptophysin and mouse
611 anti-Syt1. The other antibodies used in this study were obtained from commercial sources as
612 stated: rabbit anti-LRRK2 (ab133474, RRID: AB_2713963) from Abcam; mouse anti-α-
613 synuclein (610786, RRID: AB_2748880), mouse anti-AP2 (611350, RRID: AB_398872) and
614 mouse anti-Hip1R (612118, RRID: AB_399489) from BD Biosciences; rabbit anti-DARPP-32
615 (2306, RRID: AB_823479) from Cell Signaling Technology; mouse anti-α-adaptin (MA1-064,
616 AB_2258307) from Life Technologies; mouse anti-Amph2 (05-449, RRID: AB_309738), goat
617 anti-ChAT (AB144P, RRID: AB_2079751), mouse anti-CLC (AB9884, RRID: AB_992745), rat
618 anti-DAT (MAB369, RRID: AB_2190413), mouse anti-SV2C (MABN367, RRID: AB_2905667)
619 and rabbit anti-TH (AB152, RRID: AB_390204) from Merck Millipore; mouse anti-β-actin (sc-
620 47778, RRID: AB_2714189) and mouse anti-Hsc70 (sc-7298, RRID: AB_627761) from Santa

621 Cruz Biotechnology; rabbit anti-Auxilin (HPA031182, RRID: AB_10611957), rabbit anti-GABA
622 (A2052, RRID: AB_477652), rabbit anti-GFAP (ZRB2383, RRID: AB_2905668) and rabbit
623 anti-SJ1 (HPA011916, RRID: AB_1857692) from Sigma-Aldrich; rabbit anti-Amphiphysin 1
624 (120002, RRID: AB_887690), rabbit anti-AADC (369003, RRID: AB_2620131), rabbit anti-
625 SV2B (119102), rabbit anti-SV2C (119202, RRID: AB_887803), rabbit anti-Synaptogyrin 3
626 (103 302, RRID: AB_2619752), and rabbit anti-Syt11 (270003, RRID: AB_2619994) from
627 Synaptic Systems; rabbit anti-Iba1 (019-19741, RRID: AB_839504) from FUJIFILM Wako
628 Chemicals.
629
630 Secondary antibodies used were all purchased from commercial sources as stated: donkey
631 anti-mouse IgG (H+L) Alexa Fluor 594 (A21203, RRID: AB_141633), goat anti-mouse IgG
632 (H+L) Alexa Fluor 488 (A11001, RRID: AB_2534069), goat anti-mouse IgG (H+L) Alexa Fluor
633 594 (A11032, RRID: AB_2534091), goat anti-mouse IgG (H+L) Alexa Fluor 647 (A21236,
634 RRID: AB_2535805), donkey anti-rabbit IgG (H+L) Alexa Fluor 488 (A21206, RRID:
635 AB_2535792), goat anti-rabbit IgG (H+L) Alexa Fluor 488 (A11034, RRID: AB_2576217), goat
636 anti-rabbit IgG (H+L) Alexa Fluor 594 (A11037, RRID: AB_2534095), goat anti-rabbit IgG (H+L)
637 Alexa Fluor 647 (A21244, RRID: AB_2535812), goat anti-rat IgG (H+L) Alexa Fluor 488
638 (A11006, RRID: AB_2534074), goat anti-rat IgG (H+L) Alexa Fluor 594 (A11007, RRID:
639 AB_10561522) and donkey anti-goat IgG (H+L) Alexa Fluor 488 (A11055, RRID: AB_2534102)
640 from Life Technologies and IRDye 800CW donkey anti-rabbit IgG (926-32213, RRID:
641 AB_621848), IRDye 800CW donkey anti-mouse IgG (926-32212, RRID: AB_621847), IRDye
642 680RD donkey anti-mouse IgG (926-68072, RRID: AB_10953628) and IRDye 800CW goat
643 anti-rat (926-32219, RRID: AB_1850025) from LI-COR Biosciences.
644
645 **Motor Behavioral tests**
646 Aux-KO and littermate control mice between 2-13 months old were used for balance beam
647 and rotarod tests. The mice were divided into three age groups: 2-4 months old (n=13-15 for
648 each genotype), 5-8 months old (n=7-12) and more than 9 months old (n=8-15). Both males
649 and females were used for the behavioral assays. Both tests were conducted during the light
650 period. The mice were allowed to acclimatize to the test for at least 30 min before each test.
651 ***Balance Beam Test***
652 A narrow beam (10 mm width) was suspended 15 cm above a soft padding. Mice were placed
653 on end of the beam and during their trip towards the other end, the number of missteps (paw
654 slips) was recorded. The test was conducted thrice for each mouse and the average number
655 of missteps was calculated.
656 ***Rotarod Test***

657 Mice were placed on a rod which is rotating at 4 rpm with an acceleration to 40 rpm within 6
658 min. The duration of the mice staying on the rod is measured two times at 10 min intervals
659 and the average 'latency to fall' was determined for each mouse.
660
661 **Immunoblotting**
662 Mouse brain tissues were homogenized in buffer containing 20 mM Tris-HCl (pH 7.4), 150
663 mM NaCl, 2 mM EDTA and cOmplete™ EDTA-free Protease Inhibitor Cocktail (Roche, USA).
664 The homogenized samples were centrifuged at 700 g for 10 min to obtain the post-nuclear
665 supernatant (PNS). Protein concentration was determined by the Pierce BCA Protein Assay
666 Kit. SDS-PAGE and western blotting were performed by standard procedures. The
667 membranes were blotted with primary antibodies and then IRDye® Secondary Antibodies (LI-
668 COR, USA). The protein bands were detected using Odyssey ® CLx imaging system and its
669 intensity was quantified via Image Studio Lite software (Ver 5.2, RRID: SCR_013715). A
670 minimum of three independent sets of samples were used for quantification.
671
672 **Primary Cortical Neuron Culture and Staining**
673 Cultures of cortical neurons were prepared from P0 to P2 neonatal mouse brains by previously
674 described methods (Ferguson et al., 2007) and used at DIV19. Cortical tissue was dissected
675 out, placed in ice-cold HBSS, and diced into small pieces of less than 1 $mm^3$ per piece. Tissue
676 was then digested for 30 min in an activated enzyme solution containing papain (20 U/ml) and
677 DNase (20 µg/ml) at 37°C, followed by gentle trituration. The cell suspension is centrifuged at
678 300 g for 5 min. The cell pellet is resuspended and plated onto poly-d-lysine-coated coverslips
679 to a density of 60,000 cells/$cm^2$. 2-3 hours after plating, the medium was exchanged to
680 Neurobasal/B27 serum-free medium, and cells were maintained at 37°C in a 5% CO2
681 humidified incubator. Cells were fixed with 4% paraformaldehyde (PFA) and 4% sucrose in 1
682 X PBS for 20 min, followed by 10 min incubation with 50 mM $NH_4Cl$, then blocked and
683 permeabilized with 5% bovine serum albumin (BSA), 1 X phosphate-buffered saline (PBS)
684 and 0.1% Triton X-100. Primary and secondary antibody incubations were subsequently
685 performed in the same buffer. Alexa 488, 594 and 647 conjugated secondary antibodies were
686 purchased from Invitrogen. After washing, samples were mounted on slides with Fluoromount-
687 G (Invitrogen). Samples were observed and imaged on a spinning disk system (Gataca
688 Systems) based on an inverted microscope (Nikon Ti2-E; Nikon) equipped with a confocal
689 spinning head (CSU-W, Yokogawa) and a Plan-Apo 60x oil TIRF objective.
690
691 **Brain Histology and Immunofluorescence**
692 Mice were anesthetized with a Ketamine/Xylazine anesthetic cocktail injection, perfused
693 transcardially with ice-cold 4% PFA in 1X PBS and the brains were kept in the same fixative

694 overnight at 4°C. On the next day, brains were transferred to 30% sucrose in 1 X PBS and
695 kept overnight at 4°C on top of a roller. Brains were then embedded in OCT (Tissue-Tek) and
696 freeze in liquid nitrogen-cooled 2-methylbutane (Isopentane). Coronal or sagittal sections of
697 20 μm thickness were cut with a cryostat. The sections are either mounted on adhesive slide,
698 SuperFrost® Plus (VWR) or collected as floating sections in 1 X PBS in a 24-well plate.
699 Sections were then blocked in 5% BSA and 0.1% Triton X-100 in 1 X PBS for 1 hour at room
700 temperature. After blocking, sections were incubated with primary antibodies (diluted in the
701 same buffer) and kept overnight at 4°C. Subsequently, sections were washed 3 times for 10
702 min with 0.1% Triton X-100 in 1 X PBS, then incubated with Alexa-conjugated secondary
703 antibodies for 1 hour at room temperature. Finally, the sections were mounted with
704 Fluoromount-G (Invitrogen) and sealed with nail polish. The floating sections were mounted
705 onto slides after all the staining procedures. Images were acquired with a spinning disk system
706 (Gataca Systems) based on an inverted microscope (Nikon Ti2-E; Nikon) equipped with a
707 confocal spinning head (CSU-W, Yokogawa) and a Plan-Apo 40x oil objective.
708
709 **Quantification of Immunoreactivity Clustering and TH positive Striatal Interneurons**
710 The endocytic protein clustering quantification was conducted on the Fiji software (Version
711 ImageJ 1.52p/Java 1.8.0_172 (64-bit), RRID: SCR_002285) as follows. The same threshold
712 intensity was applied to all images and a random region of interest with an area of 500 $\mu m^2$
713 was manually selected. A mask was used to selectively quantify puncta larger than 1 $\mu m^2$.
714 The Fiji plugin "Analyze particles" was then used to measure average fluorescence intensity
715 of the puncta. The quantification of TH and DAT positive clustering in striatum was also done
716 similarly using Fiji software. In this case, for each mouse, 5 random sampling sites were
717 selected respectively for both dorsal and ventral striatum. At least three mice from each
718 genotype and each age group were collected for this purpose. The threshold setting for the
719 clusters was set to quantify puncta bigger than 5 $\mu m^2$ to ensure normal positive axonal
720 terminals were not counted in. The average size of clusters and average number of clusters
721 was counted automatically with Fiji plugin "Analyse Particles" based on all five random
722 sampling sites for each mouse.
723
724 Quantification of the THINs were done with the same images used to quantify TH/DAT positive
725 clusters. The number of TH positive cell bodies were counted from the 5 random sampling
726 sites selected for the dorsal and ventral striatum respectively.
727
728 **Quantification of Striatal Cholinergic Interneurons (ChINs)**
729 The number of ChINs was quantified from individual coronal sections of the striatum double
730 stained with ChAT and SV2C. Image acquisition involved tiling of the entire section using a

731 20x Air lens, keeping the same laser intensity and exposure for both channels. Stitched
732 images were then set to the same threshold intensity for each individual channel in Fiji. Cell
733 Counter plugin was used to count visible cell bodies across the striatum (outlined on the basis
734 of Allen mouse brain atlas). Percentage ratio of the cell count from individual channels was
735 used as a measure of ChINs upregulating SV2C.
736
737 Quantification of ChAT and SV2C intensities in ChINs was done with the same images used
738 for quantifying number of cholinergic interneurons. Manually drawn ROIs were used to analyse
739 the intensities of 20 neurons randomly selected across the striatum. Corrected total cell
740 fluorescence (CTCF) was calculated and the intensities of each channel were normalised to
741 control levels. For both genotypes, three individual mice were analysed for this purpose.
742
743 **Electron Microscopy (EM)**
744 All EM reagents were from EMS, Hatfield, PA, unless noted otherwise. 1-3 months old mice
745 were anesthetized and fixed by transcardial perfusion with 4% formaldehyde and 0.125%
746 glutaraldehyde in 0.1 M PB buffer. Brain were removed and dissected in small pieces (0.5 ×
747 0.5 x 0.5 $mm^3$) and further incubated in the same fixative at 4 °C overnight. Brain tissues were
748 further incubated in 2.5% glutaraldehyde in 0.1 M sodium cacodylate buffer for additional 1
749 hour at room temperature, post-fixed (1 hour) in 2% OsO4, 1.5% K4Fe(CN)6 (Sigma-Aldrich,
750 St. Louis, MO) in 0.1M sodium cacodylate buffer, stained (overnight) with 2% aqueous uranyl
751 acetate at 4 °C, dehydrated in gradually increasing concentration of EtoH, and embedded in
752 Embed 812. Ultrathin sections, about 60 nm thick, were cut with a Leica ultramicrotome and
753 examined in a Talos L120C TEM microscope at 80 kV. Images were taken with Velox software
754 and a 4k × 4K Ceta CMOS Camera (Thermo Fisher Scientific). For quantification, images of
755 synapses were selected based on the presence of an active zone. The number of SVs
756 (diameter ≤ 80nm), CCVs, and clathrin cages was measured in more than 120 synapses for
757 each control and mutant condition. These values were normalized to the cross-sectional area
758 of the presynaptic terminal. Results of the morphometric analysis are presented as mean ±
759 SD. Statistical significance was evaluated using one-way ANOVA followed by Games-
760 Howell's multiple comparison test.
761
762 **Immunogold labeling**
763 Aux-KO/ SJ1-$KI^{RQ}$ mice were transcardially perfused with 4% formaldehyde and 0.125%
764 glutaraldehyde in 0.1M phosphate buffer (pH 7.4). Dorsal striata were dissected and
765 embedded in 1% gelatin in 0.1M phosphate buffer. Tissue pieces were trimmed, infiltrated in
766 2.3M sucrose, and then were frozen rapidly onto aluminum pins in liquid nitrogen. 60nm frozen

767 sections on carbon/formvar coated grids were prepared with a Leica Cryo-EMUC6 UltraCut
768 microtome. Sections were labelled with rabbit anti-Tyrosine Hydroxylase (TH) and 10nm
769 Protein A gold (Utrecht Medical Center) (Tokuyasu K.T., 1973). Grids were examined in FEI
770 Tecnai Biotwin TEM at 80Kv. Images were taken with Morada CCD and iTEM (Olympus)
771 software.
772
773 **Statistical Analysis**
774 All statistical analysis was performed using GraphPad Prism (Ver 9.3.1, RRID: SCR_002798).
775 All graphs were also plotted on GraphPad Prism. Data are presented as mean ± SEM unless
776 otherwise stated. Statistical significance was determined using the Student's unpaired *t* test
777 for the comparison of two independent groups or ANOVA with Tukey's Honest Significant
778 Difference or Games-Howell's post hoc test for multiple group comparisons. Data with *p*-
779 values <0.05, <0.01, <0.001, and <0.0001 are represented by asterisks *, **, ***, and ****.
780 Refer to figures for exact *p*-values.
781
782
783 **Acknowledgment**
784 We thank Morven Graham for technical help and Prof. Zhang Su-Chun for sharing the
785 reagents. This research was supported in part by grants from Ministry of Education Academic
786 Research Fund (AcRF) Tier 2 Singapore (MOE2019-T2-2-090) to MC, from the NIH (NS36251
787 and DA18343), the Kavli Institute for Neuroscience, the Parkinson Foundation and the
788 Aligning Science Across Parkinson's grant ASAP-000580 through the Michael J. Fox
789 Foundation for Parkinson's Research (MJFF) to PDC. For the purpose of open access, the
790 author has applied a CC BY public copyright license to all Author Accepted Manuscripts arising
791 from this submission.
792
793 **Author Contributions**
794 X.Y.N., P.D.C. and M.C. designed the experiments. X.Y.N., Y.W., Y.L., S.M.Y and M.C.
795 performed the experiments. X.Y.N., P.D.C. and M.C. wrote the paper. L.E.G. provided Aux-
796 KO mice. All authors read and approved the final manuscript.
797
798 **Competing interests**
799 The authors declare no competing interests. Pietro De Camilli is a member of the Scientific
800 Advisory Board of CASMA Therapeutics.
801
802
803 **Supplementary Figure Legends**

804

805 **Supplementary Figure 1. Aux-KO/SJ1-KI$^{RQ}$ mice are smaller in size but have normal**
806 **brain development and architecture.**
807 (a-b) Image of the size of P25 Aux-KO/ SJ1-KI$^{RQ}$ mice comparing with its littermate single
808 mutants; (a) Aux-KO and (b) SJ1-KI$^{RQ}$.
809 (c) H&E staining reveals absence of gross structural abnormality in various regions (cortex,
810 hippocampus, striatum and cerebellum) of 1-month-old SJ1-KI$^{RQ}$, Aux-KO and Aux-KO/SJ1-
811 KI$^{RQ}$ mice brain.
812

813 **Supplementary Figure 2. Absence of gliosis in Aux-KO/SJ1-KI$^{RQ}$ brain**
814 (a and b) No obvious difference in immunostaining intensity of (a) Iba1-microglia marker and
815 (b) GFAP-astrocytes marker in different regions of 1-month-old Ctrl, SJ1-KI$^{RQ}$, Aux-KO and
816 Aux-KO/SJ1-KI$^{RQ}$ mice brain.
817

818 **Supplementary Figure 3. Western blot analysis of endocytic proteins, synaptic proteins,**
819 **DAergic markers and PD-related proteins in mouse brains.**
820 (a) Representative blots for various proteins involved in PD and synaptic endocytosis from 1-
821 month-old control, SJ1-KI$^{RQ}$, Aux-KO and Aux-KO/ SJ1-KI$^{RQ}$ whole brain homogenates.
822 (b) Quantification of expression levels of the proteins shown in (a). Protein levels were
823 normalized to the level of Actin. Data are represented as mean ± SEM (* $p<0.05$, ** $p<0.005$,
824 and *** $p<0.001$, by one-way ANOVA with post-hoc Tukey's test). Ctrl: n=3, Aux-KO: n=4,
825 SJ1-KI$^{RQ}$: n=3, and Aux-KO/SJ1-KI$^{RQ}$: n=4.
826

827 **Supplementary Figure 4. Presence of dystrophic changes only in the axon terminals of**
828 **DAergic neurons but not the cell bodies of Aux-KO/SJ1-KI$^{RQ}$ mice.**
829 (a) Double staining of anti-TH and anti-AADC showed normal morphology of DAergic neuron
830 cell bodies and dendrites in the midbrain.
831 (b) AADC (green) and DAT (red) immunostaining reveals the presence of AADC/DAT+
832 aggregates in the olfactory tubercle (OT, part of ventral striatum) of Aux-KO/SJ1-KI$^{RQ}$ mice.
833

834 **Supplementary figure 5. Overview of cluster distribution in the striatum of Aux-KO, SJ1-**
835 **KI$^{RQ}$ and Aux-KO/SJ1-KI$^{RQ}$ mice.**
836 Tiling of a single coronal striatum section immunostained for DAT. White dotted line separates
837 the dorsal and ventral striatum of the mice. Insets on the bottom left corner of the image
838 showed high magnification images of the clusters for dorsal (pink, top) and ventral (purple,
839 bottom) striatum for each genotype. Note the absence of clusters in the ventral striatum in all

840 mice except the Aux-KO/SJ1-KI$^{RQ}$ mice. Bottom right inset of the Aux-KO tiling image depicts
841 the dorsal (pink) and ventral (purple) mouse striatum.
842
843 **Supplementary figure 6. EM immunogold labelling of onion-like membrane structure in**
844 **dorsal striatum of Aux-KO/SJ1-KI$^{RQ}$ mice.**
845 Anti-TH immunogold labelling (10 nm gold particles) of an ultrathin frozen sections of
846 AuxKO/SJ1-KI$^{RQ}$ dorsal striatum. The multilayered membrane structures are positive for TH
847 immunoreactivity.
848
849 **Supplementary figure 7. Various other markers examined with TH/ DAT positive**
850 **clusters**
851 (a-b) Representative images for immunoreactivity of anti-DAT or TH with (a) anti-AADC and
852 (b) anti-SV2C in Aux-KO and SJ1-KI$^{RQ}$ mice.
853 (c) Immunostaining of DAT with Syt1 showed partial colocalization in Aux-KO/SJ1-KI$^{RQ}$ double
854 mutant striatum.
855 (d-g) Double immunofluorescence of synapsin, GFAP, Iba1 and Darpp32 with TH/ DAT
856 showed no colocalization in the striatum of Aux-KO/SJ1-KI$^{RQ}$ mice.
857
858 **Supplementary figure 8. Immunofluorescence analysis of SNAP25 in different brain**
859 **regions.**
860 (a) Immunostaining of SNAP25 (green) showed partial colocalization with DAT positve
861 clusters (red) in the striatum of Aux-KO, SJ1-KI$^{RQ}$ and Aux-KO/SJ1-KI$^{RQ}$ mice.
862 (b) Immunoreactivity of anti-SNAP25 in the cortex of WT, Aux-KO, SJ1-KI$^{RQ}$ and Aux-KO/SJ1-
863 KI$^{RQ}$ mice. No clusters of SNAP25 were observed in the cortex.
864
865 **Supplementary figure 9. Properties of striatal THINs and ChINs in the striatum of Aux-**
866 **KO/SJ1-KI$^{RQ}$ mice.**
867 (a) Immunoreactivity of anti-TH with anti-Darpp32 showed that THINs is a distinct group of
868 neurons from Darpp32 positive MSNs.
869 (b) Double staining of anti-TH and anti-GABA showed that THINs are GABAergic striatal
870 interneurons.
871 (c-d) Immunostaining of SV2C using a different anti-SV2C antibody (host species: Rabbit)
872 labelled the same structures: (c) ChAT-positive ChINs and (d) SV2C/DAT positive clusters in
873 Aux-KO/SJ1-KI$^{RQ}$.
874 (e-f) A large microscope field of view showed the distribution of (e) SV2C positive and (f) ChAT
875 positive interneurons in the striatum of WT and Aux-KO/SJ1-KI$^{RQ}$ mice.
876

**Supplementary figure 10. More severe DA dystrophic phenotype in 7-month-old AuxKO/SJ1-KI$^{RQ}$ mice**

Representative images for double immunofluorescence of TH/DAT, AADC/DAT and SV2C/DAT for all 4 genotypes at 7-month-old. The only Aux-KO/SJ1-KI$^{RQ}$ that managed to survive till this age showed increased number of clusters, THINs and ChINs compared to the other 3 genotypes.

**Supplementary Video Legends**

**Supplementary Video 1 Tonic-clonic epileptic seizures in a 5-month-old Aux-KO mouse.**

**Supplementary Video 2 Balance beam test in 2-month-old (a) Ctrl and (b) Aux-KO mice.**

**Supplementary Video 3 Balance beam test in 4-month-old (a) Ctrl, (b) Aux-KO/SJ1-WT, (c) Aux-Ht/SJ1-KI$^{RQ}$ and (d) Aux-KO/SJ1-KI$^{RQ}$ mice.** This 4-month-old Aux-KO/SJ1-KI$^{RQ}$ mouse is the same mouse that managed to survive till 7-month-old.

**Reference**


1 Blauwendraat, C., Nalls, M. A. & Singleton, A. B. The genetic architecture of Parkinson's disease. *Lancet Neurol* **19**, 170-178, doi:10.1016/S1474-4422(19)30287-X (2020).

2 Bandres-Ciga, S., Diez-Fairen, M., Kim, J. J. & Singleton, A. B. Genetics of Parkinson's disease: An introspection of its journey towards precision medicine. *Neurobiol Dis* **137**, 104782, doi:10.1016/j.nbd.2020.104782 (2020).

3 Pirooznia, S. K., Rosenthal, L. S., Dawson, V. L. & Dawson, T. M. Parkinson Disease: Translating Insights from Molecular Mechanisms to Neuroprotection. *Pharmacol Rev* **73**, 33-97, doi:10.1124/pharmrev.120.000189 (2021).

4 Tagliaferro, P. & Burke, R. E. Retrograde Axonal Degeneration in Parkinson Disease. *J Parkinsons Dis* **6**, 1-15, doi:10.3233/JPD-150769 (2016).

5 Abeliovich, A. & Gitler, A. D. Defects in trafficking bridge Parkinson's disease pathology and genetics. *Nature* **539**, 207-216, doi:10.1038/nature20414 (2016).

6 Quadri, M. *et al.* Mutation in the SYNJ1 gene associated with autosomal recessive, early-onset Parkinsonism. *Human mutation* **34**, 1208-1215, doi:10.1002/humu.22373 (2013).

7 Krebs, C. E. *et al.* The Sac1 domain of SYNJ1 identified mutated in a family with early-onset progressive Parkinsonism with generalized seizures. *Human mutation* **34**, 1200-1207, doi:10.1002/humu.22372 (2013).

8 Edvardson, S. *et al.* A deleterious mutation in DNAJC6 encoding the neuronal-specific clathrin-uncoating co-chaperone auxilin, is associated with juvenile parkinsonism. *PloS one* **7**, e36458, doi:10.1371/journal.pone.0036458 (2012).

9 Koroglu, C., Baysal, L., Cetinkaya, M., Karasoy, H. & Tolun, A. DNAJC6 is responsible for juvenile parkinsonism with phenotypic variability. *Parkinsonism Relat Disord* **19**, 320-324, doi:10.1016/j.parkreldis.2012.11.006 (2013).

10 Nguyen, M., Wong, Y. C., Ysselstein, D., Severino, A. & Krainc, D. Synaptic, Mitochondrial, and Lysosomal Dysfunction in Parkinson's Disease. *Trends Neurosci* **42**, 140-149, doi:10.1016/j.tins.2018.11.001 (2019).

11 Saheki, Y. & De Camilli, P. Synaptic vesicle endocytosis. *Cold Spring Harbor perspectives in biology* **4**, a005645, doi:10.1101/cshperspect.a005645 (2012).
12 Guan, R., Dai, H., Harrison, S. C. & Kirchhausen, T. Structure of the PTEN-like region of auxilin, a detector of clathrin-coated vesicle budding. *Structure* **18**, 1191-1198, doi:10.1016/j.str.2010.06.016 (2010).
13 Dyment, D. A. *et al.* Homozygous nonsense mutation in SYNJ1 associated with intractable epilepsy and tau pathology. *Neurobiology of aging* **36**, 1222 e1221-1225, doi:10.1016/j.neurobiolaging.2014.09.005 (2015).
14 Cremona, O. *et al.* Essential role of phosphoinositide metabolism in synaptic vesicle recycling. *Cell* **99**, 179-188, doi:S0092-8674(00)81649-9 [pii] (1999).
15 Ng, J. *et al.* DNAJC6 Mutations Disrupt Dopamine Homeostasis in Juvenile Parkinsonism-Dystonia. *Mov Disord* **35**, 1357-1368, doi:10.1002/mds.28063 (2020).
16 Lesage, S. *et al.* Clinical Variability of SYNJ1-Associated Early-Onset Parkinsonism. *Front Neurol* **12**, 648457, doi:10.3389/fneur.2021.648457 (2021).
17 Gao, X. *et al.* Multimodal analysis of gene expression from postmortem brains and blood identifies synaptic vesicle trafficking genes to be associated with Parkinson's disease. *Brief Bioinform*, doi:10.1093/bib/bbaa244 (2020).
18 Pan, P. Y. *et al.* Synj1 haploinsufficiency causes dopamine neuron vulnerability and alpha-synuclein accumulation in mice. *Hum Mol Genet* **29**, 2300-2312, doi:10.1093/hmg/ddaa080 (2020).
19 Farrow, S. L. *et al.* Establishing gene regulatory networks from Parkinson's disease risk loci. *Brain*, doi:10.1093/brain/awac022 (2022).
20 Olgiati, S. *et al.* DNAJC6 Mutations Associated With Early-Onset Parkinson's Disease. *Ann Neurol* **79**, 244-256, doi:10.1002/ana.24553 (2016).
21 Cao, M. *et al.* Parkinson Sac Domain Mutation in Synaptojanin 1 Impairs Clathrin Uncoating at Synapses and Triggers Dystrophic Changes in Dopaminergic Axons. *Neuron* **93**, 882-896 e885, doi:10.1016/j.neuron.2017.01.019 (2017).
22 Yang, S. *et al.* Presynaptic autophagy is coupled to the synaptic vesicle cycle via ATG-9. *Neuron*, doi:10.1016/j.neuron.2021.12.031 (2022).
23 Vanhauwaert, R. *et al.* The SAC1 domain in synaptojanin is required for autophagosome maturation at presynaptic terminals. *EMBO J* **36**, 1392-1411, doi:10.15252/embj.201695773 (2017).
24 Cao, M., Park, D., Wu, Y. & De Camilli, P. Absence of Sac2/INPP5F enhances the phenotype of a Parkinson's disease mutation of synaptojanin 1. *Proc Natl Acad Sci U S A* **117**, 12428-12434, doi:10.1073/pnas.2004335117 (2020).
25 Song, L. *et al.* Auxilin Underlies Progressive Locomotor Deficits and Dopaminergic Neuron Loss in a Drosophila Model of Parkinson's Disease. *Cell Rep* **18**, 1132-1143, doi:10.1016/j.celrep.2017.01.005 (2017).
26 Yim, Y. I. *et al.* Endocytosis and clathrin-uncoating defects at synapses of auxilin knockout mice. *Proc Natl Acad Sci U S A* **107**, 4412-4417, doi:10.1073/pnas.1000738107 (2010).
27 Roosen, D. A. *et al.* Mutations in Auxilin cause parkinsonism via impaired clathrin-mediated trafficking at the Golgi apparatus and synapse. *bioRxiv*, 830802, doi:10.1101/830802 (2021).
28 Wulansari, N. *et al.* Neurodevelopmental defects and neurodegenerative phenotypes in human brain organoids carrying Parkinson's disease-linked DNAJC6 mutations. *Sci Adv* **7**, doi:10.1126/sciadv.abb1540 (2021).
29 Dunn, A. R. *et al.* Synaptic vesicle glycoprotein 2C (SV2C) modulates dopamine release and is disrupted in Parkinson disease. *Proc Natl Acad Sci U S A* **114**, E2253-E2262, doi:10.1073/pnas.1616892114 (2017).
30 Janz, R. & Sudhof, T. C. SV2C is a synaptic vesicle protein with an unusually restricted localization: anatomy of a synaptic vesicle protein family. *Neuroscience* **94**, 1279-1290, doi:10.1016/s0306-4522(99)00370-x (1999).

31 Foo, J. N. *et al.* Identification of Risk Loci for Parkinson Disease in Asians and Comparison of Risk Between Asians and Europeans: A Genome-Wide Association Study. *JAMA Neurol* **77**, 746-754, doi:10.1001/jamaneurol.2020.0428 (2020).
32 Grover, S. *et al.* Replication of a Novel Parkinson's Locus in a European Ancestry Population. *Mov Disord* **36**, 1689-1695, doi:10.1002/mds.28546 (2021).
33 Nalls, M. A. *et al.* Large-scale meta-analysis of genome-wide association data identifies six new risk loci for Parkinson's disease. *Nat Genet* **46**, 989-993, doi:10.1038/ng.3043 (2014).
34 Luthi, A. *et al.* Synaptojanin 1 contributes to maintaining the stability of GABAergic transmission in primary cultures of cortical neurons. *J Neurosci* **21**, 9101-9111 (2001).
35 Hayashi, M. *et al.* Cell- and stimulus-dependent heterogeneity of synaptic vesicle endocytic recycling mechanisms revealed by studies of dynamin 1-null neurons. *Proc Natl Acad Sci U S A* **105**, 2175-2180, doi:10.1073/pnas.0712171105 (2008).
36 Picillo, M., Ranieri, A., Orefice, G., Bonifati, V. & Barone, P. Clinical progression of SYNJ1-related early onset atypical parkinsonism: 3-year follow up of the original Italian family. *J Neurol* **261**, 823-824, doi:10.1007/s00415-014-7270-6 (2014).
37 Li, J., Kim, S., Pappas, S. S. & Dauer, W. T. CNS critical periods: implications for dystonia and other neurodevelopmental disorders. *JCI Insight* **6**, doi:10.1172/jci.insight.142483 (2021).
38 Keber, U. *et al.* Striatal tyrosine hydroxylase-positive neurons are associated with L-DOPA-induced dyskinesia in hemiparkinsonian mice. *Neuroscience* **298**, 302-317, doi:10.1016/j.neuroscience.2015.04.021 (2015).
39 Betarbet, R. *et al.* Dopaminergic neurons intrinsic to the primate striatum. *J Neurosci* **17**, 6761-6768 (1997).
40 Doucet-Beaupre, H. *et al.* Lmx1a and Lmx1b regulate mitochondrial functions and survival of adult midbrain dopaminergic neurons. *Proc Natl Acad Sci U S A* **113**, E4387-4396, doi:10.1073/pnas.1520387113 (2016).
41 Xenias, H. S., Ibanez-Sandoval, O., Koos, T. & Tepper, J. M. Are striatal tyrosine hydroxylase interneurons dopaminergic? *J Neurosci* **35**, 6584-6599, doi:10.1523/JNEUROSCI.0195-15.2015 (2015).
42 Dunn, A. R. *et al.* Immunochemical analysis of the expression of SV2C in mouse, macaque and human brain. *Brain Res* **1702**, 85-95, doi:10.1016/j.brainres.2017.12.029 (2019).
43 Dardou, D. *et al.* Distribution of SV2C mRNA and protein expression in the mouse brain with a particular emphasis on the basal ganglia system. *Brain Res* **1367**, 130-145, doi:10.1016/j.brainres.2010.09.063 (2011).
44 Dardou, D. *et al.* A role for Sv2c in basal ganglia functions. *Brain Res* **1507**, 61-73, doi:10.1016/j.brainres.2013.02.041 (2013).
45 Tanimura, A. *et al.* Striatal cholinergic interneurons and Parkinson's disease. *Eur J Neurosci* **47**, 1148-1158, doi:10.1111/ejn.13638 (2018).
46 Hill-Burns, E. M. *et al.* A genetic basis for the variable effect of smoking/nicotine on Parkinson's disease. *Pharmacogenomics J* **13**, 530-537, doi:10.1038/tpj.2012.38 (2013).

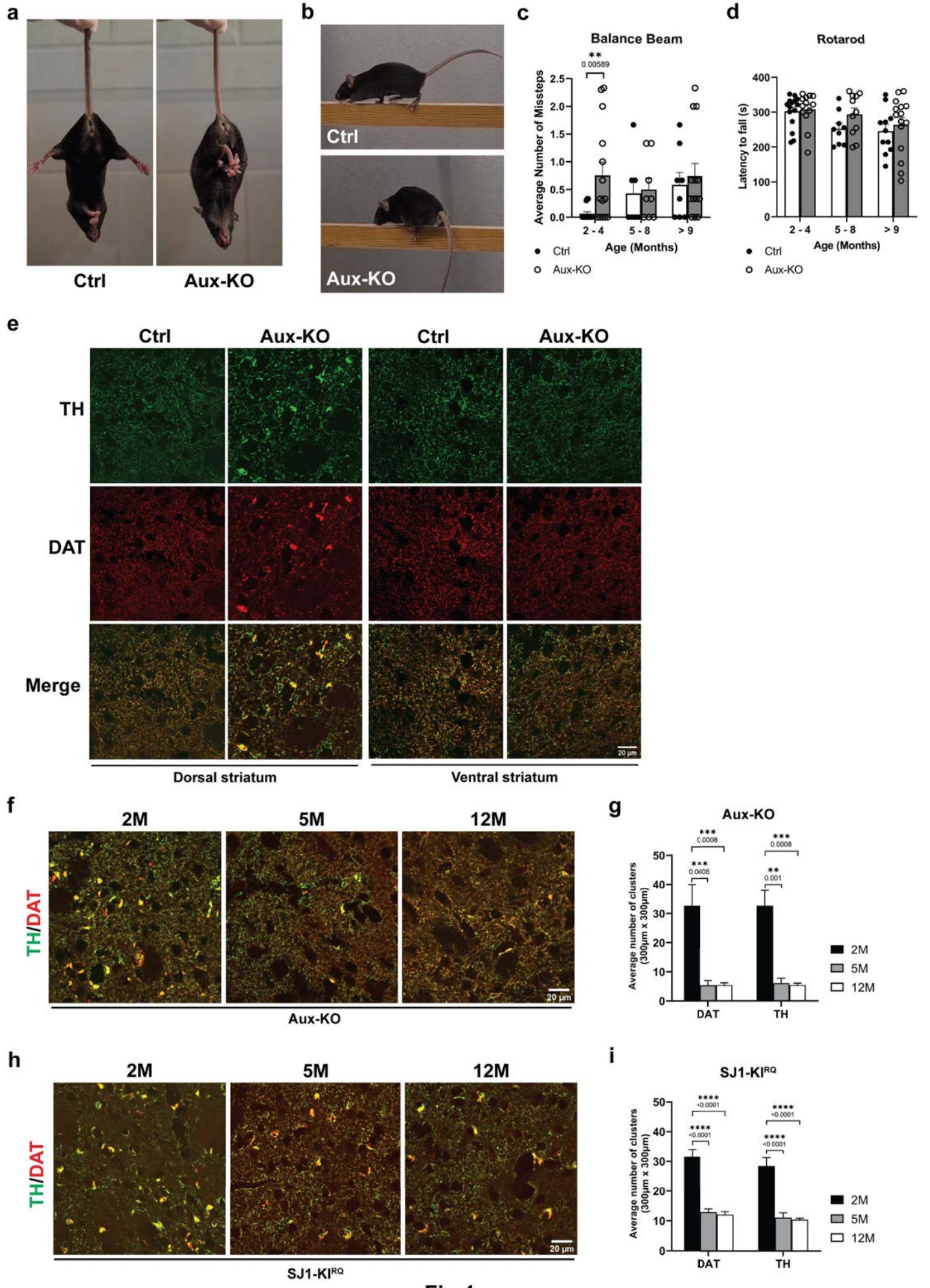
a
Ctrl
Aux-KO
b
Ctrl
Aux-KO
c
Balance Beam
**
0.00589
Average Number of Missteps
2.5
2.0
1.5
1.0
0.5
0.0
2 - 4
5 - 8
> 9
Age (Months)
Ctrl
Aux-KO
d
Rotarod
Latency to fall (s)
400
300
200
100
0
2 - 4
5 - 8
> 9
Age (Months)
Ctrl
Aux-KO
e
Ctrl
Aux-KO
Ctrl
Aux-KO
TH
DAT
Merge
20 µm
Dorsal striatum
Ventral striatum
f
2M
5M
12M
TH/DAT
20 µm
Aux-KO
g
Aux-KO
***
0.0008
***
0.0008
***
0.0008
**
0.001
Average number of clusters
(300µm x 300µm)
50
40
30
20
10
0
DAT
TH
2M
5M
12M
h
2M
5M
12M
TH/DAT
20 µm
SJ1-KI^RQ
i
SJ1-KI^RQ
****
<0.0001
****
<0.0001
****
<0.0001
****
<0.0001
Average number of clusters
(300µm x 300µm)
50
40
30
20
10
0
DAT
TH
2M
5M
12M

Fig 1

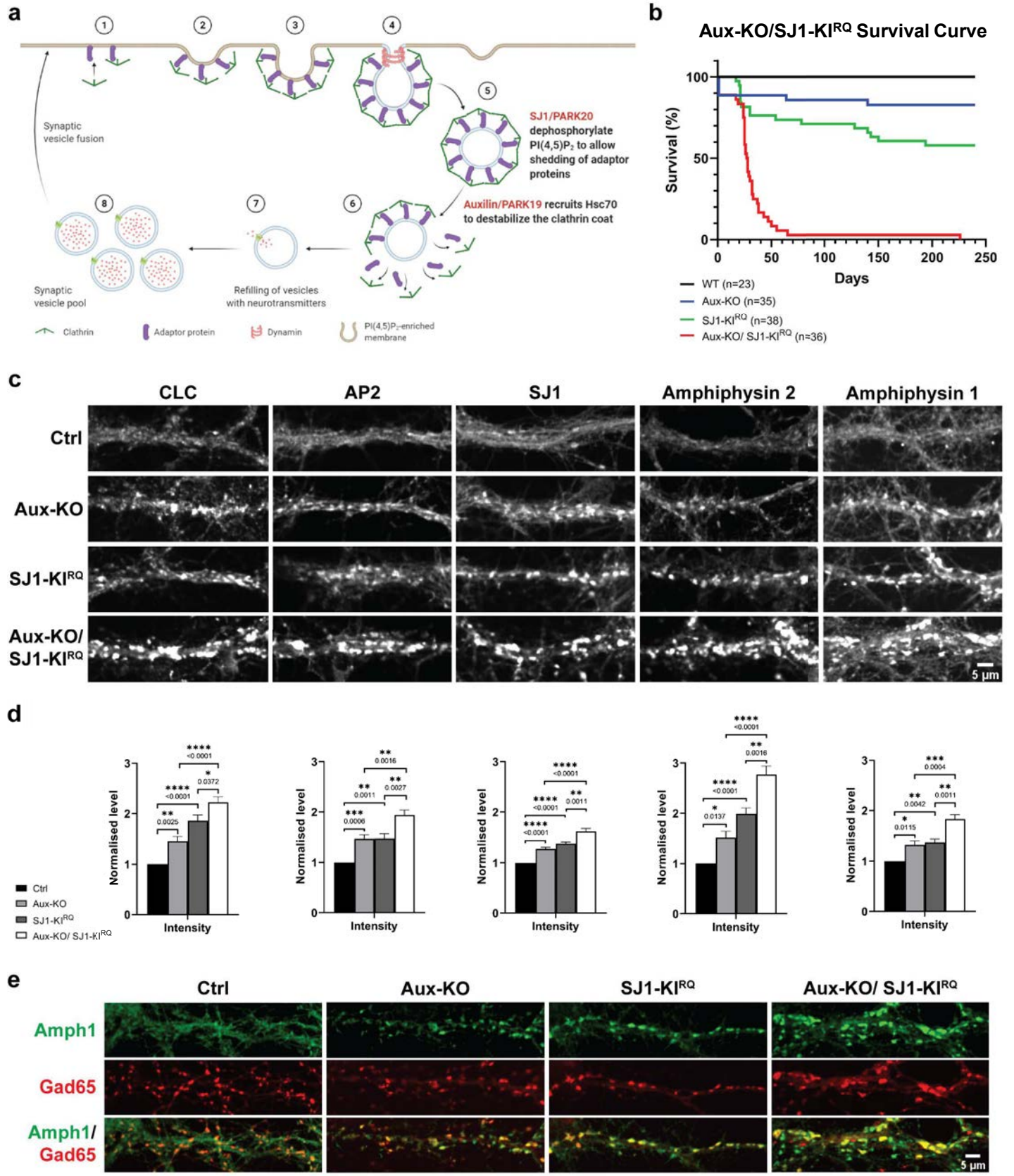
a
Synaptic vesicle fusion
SJ1/PARK20 dephosphorylate PI(4,5)P2 to allow shedding of adaptor proteins
Auxilin/PARK19 recruits Hsc70 to destabilize the clathrin coat
Synaptic vesicle pool
Refilling of vesicles with neurotransmitters
Clathrin
Adaptor protein
Dynamin
PI(4,5)P2-enriched membrane
b
Aux-KO/SJ1-KIRQ Survival Curve
Survival (%)
Days
WT (n=23)
Aux-KO (n=35)
SJ1-KIRQ (n=38)
Aux-KO/ SJ1-KIRQ (n=36)
c
CLC
AP2
SJ1
Amphiphysin 2
Amphiphysin 1
Ctrl
Aux-KO
SJ1-KIRQ
Aux-KO/ SJ1-KIRQ
5 µm
d
Normalised level
Intensity
Ctrl
Aux-KO
SJ1-KIRQ
Aux-KO/ SJ1-KIRQ
e
Ctrl
Aux-KO
SJ1-KIRQ
Aux-KO/ SJ1-KIRQ
Amph1
Gad65
Amph1/ Gad65
5 µm

Fig 2

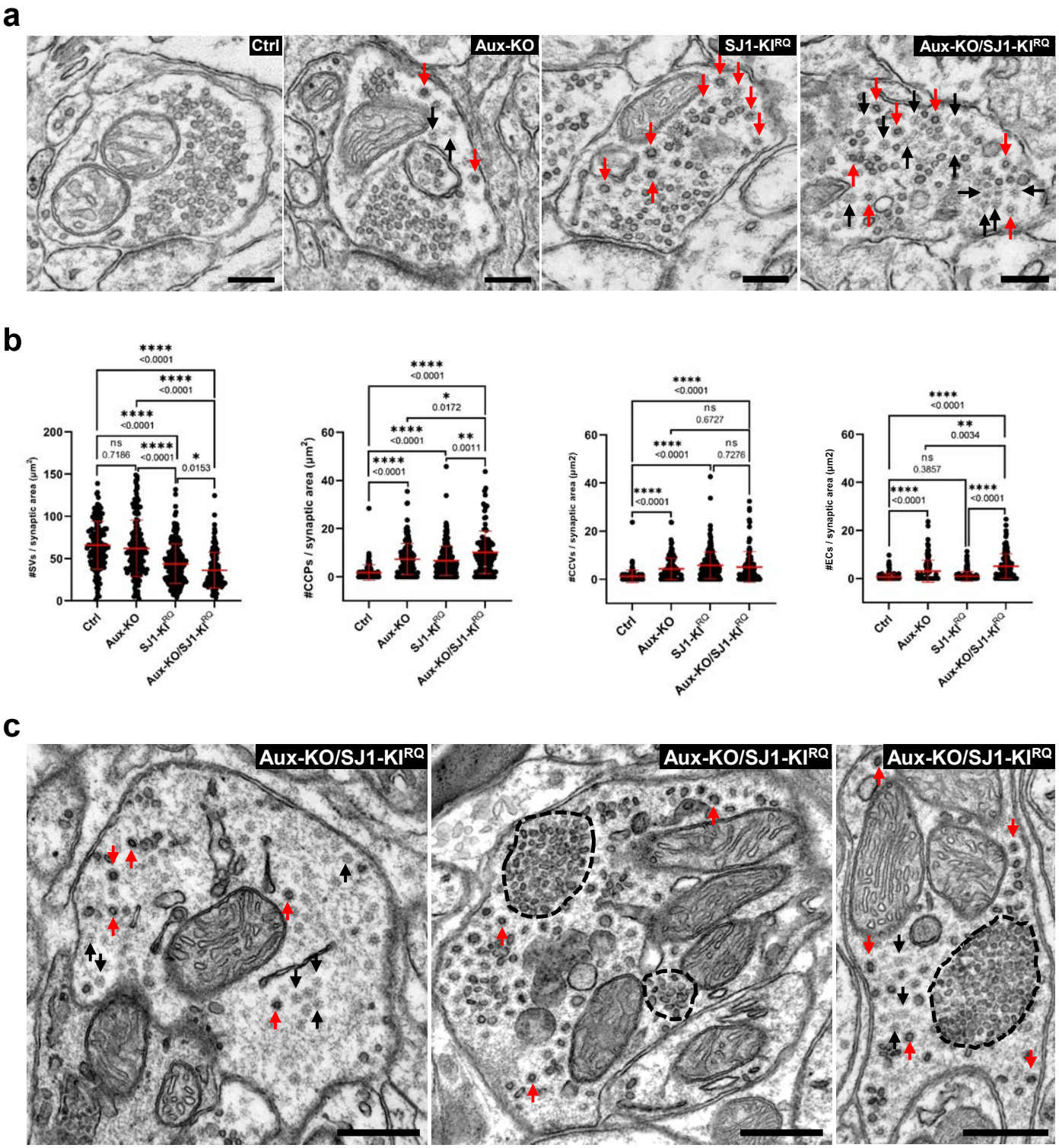
a
Ctrl
Aux-KO
SJ1-KI^RQ
Aux-KO/SJ1-KI^RQ
b
#SVs / synaptic area (µm²)
#CCPs / synaptic area (µm²)
#CCVs / synaptic area (µm2)
#ECs / synaptic area (µm2)
Ctrl
Aux-KO
SJ1-KI^RQ
Aux-KO/SJ1-KI^RQ
****
<0.0001
ns
0.7186
*
0.0153
**
0.0011
0.0172
ns
0.6727
0.7276
0.3857
0.0034
c
Aux-KO/SJ1-KI^RQ

Fig 3

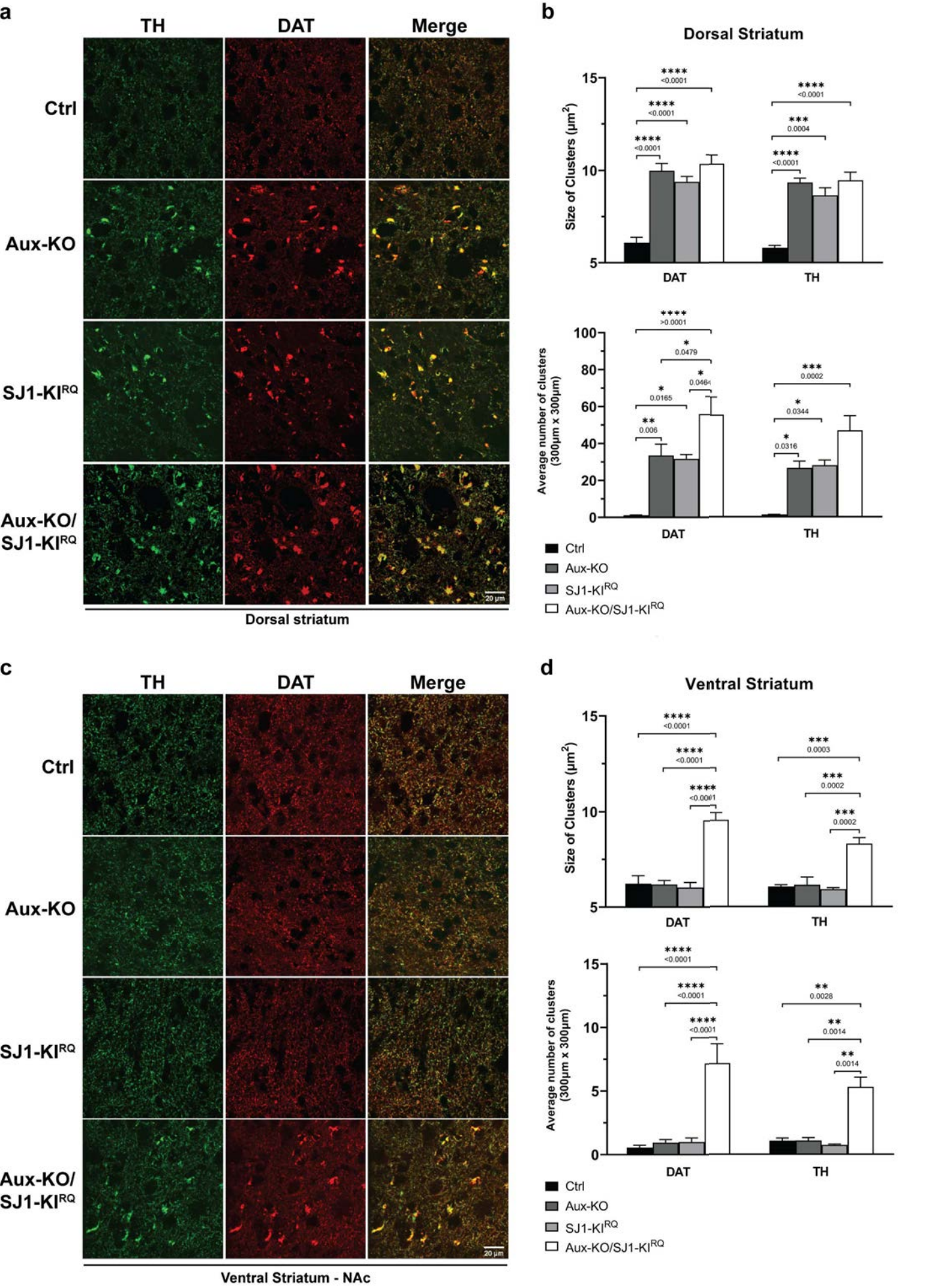
a
TH
DAT
Merge
Ctrl
Aux-KO
SJ1-KI^RQ
Aux-KO/
SJ1-KI^RQ
20 µm
Dorsal striatum
b
Dorsal Striatum
Size of Clusters (µm²)
Average number of clusters (300µm x 300µm)
DAT
TH
Ctrl
Aux-KO
SJ1-KI^RQ
Aux-KO/SJ1-KI^RQ
c
TH
DAT
Merge
Ctrl
Aux-KO
SJ1-KI^RQ
Aux-KO/
SJ1-KI^RQ
20 µm
Ventral Striatum - NAc
d
Ventral Striatum
Size of Clusters (µm²)
Average number of clusters (300µm x 300µm)
DAT
TH
Ctrl
Aux-KO
SJ1-KI^RQ
Aux-KO/SJ1-KI^RQ

Fig 4

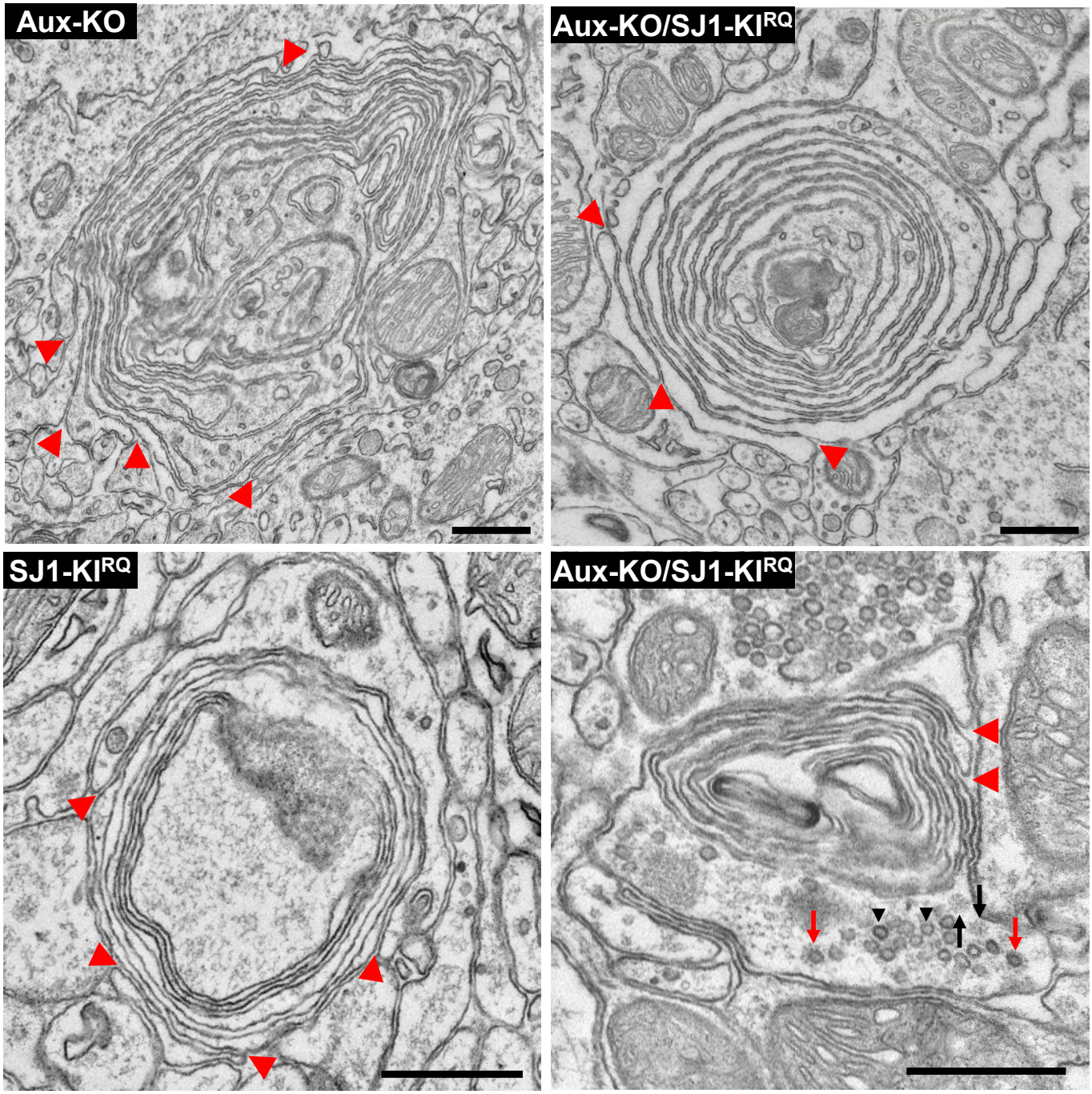


Fig 5

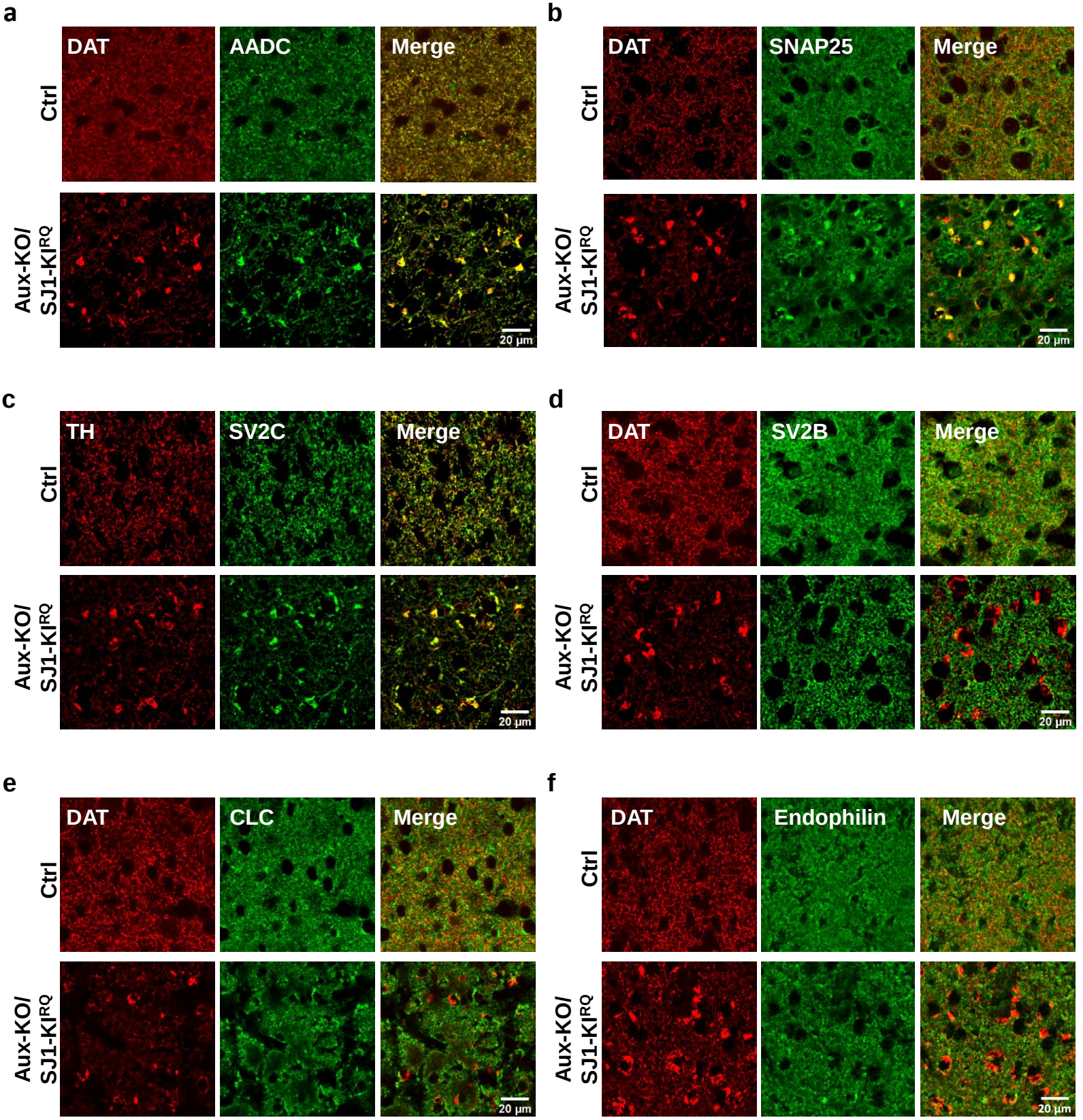
a
DAT
AADC
Merge
Ctrl
Aux-KO/
SJ1-KI^RQ
20 µm
b
DAT
SNAP25
Merge
Ctrl
Aux-KO/
SJ1-KI^RQ
20 µm
c
TH
SV2C
Merge
Ctrl
Aux-KO/
SJ1-KI^RQ
20 µm
d
DAT
SV2B
Merge
Ctrl
Aux-KO/
SJ1-KI^RQ
20 µm
e
DAT
CLC
Merge
Ctrl
Aux-KO/
SJ1-KI^RQ
20 µm
f
DAT
Endophilin
Merge
Ctrl
Aux-KO/
SJ1-KI^RQ
20 µm

Fig 6

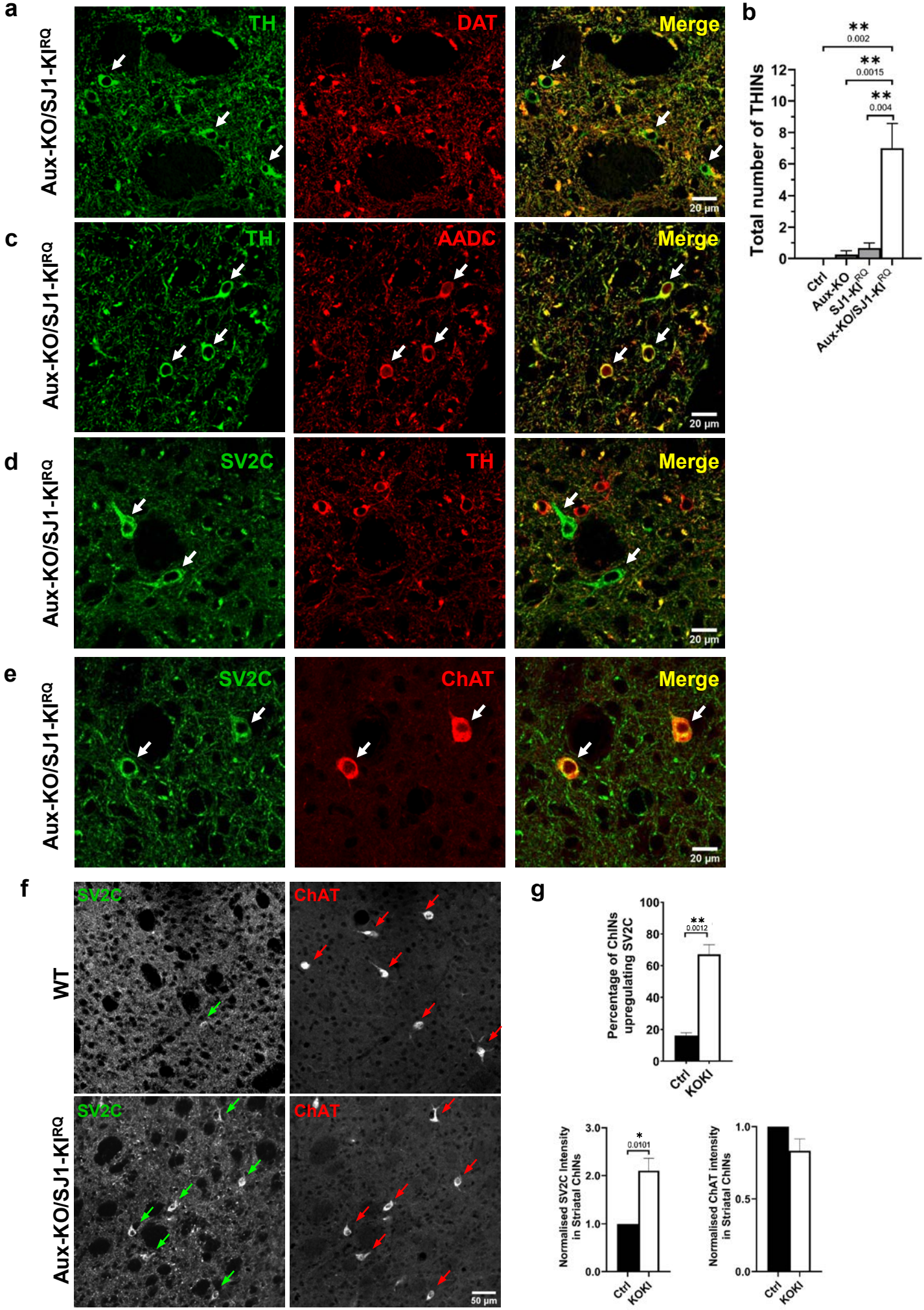
a
Aux-KO/SJ1-KI$^{RQ}$
TH
DAT
Merge
20 µm
b
Total number of THINs
**
0.002
**
0.0015
**
0.004
Ctrl
Aux-KO
SJ1-KI$^{RQ}$
Aux-KO/SJ1-KI$^{RQ}$
c
Aux-KO/SJ1-KI$^{RQ}$
TH
AADC
Merge
20 µm
d
Aux-KO/SJ1-KI$^{RQ}$
SV2C
TH
Merge
20 µm
e
Aux-KO/SJ1-KI$^{RQ}$
SV2C
ChAT
Merge
20 µm
f
WT
Aux-KO/SJ1-KI$^{RQ}$
SV2C
ChAT
50 µm
g
Percentage of ChINs upregulating SV2C
**
0.0012
Ctrl
KOKI
Normalised SV2C Intensity in Striatal ChINs
*
0.0101
Normalised ChAT intensity in Striatal ChINs

Fig 7

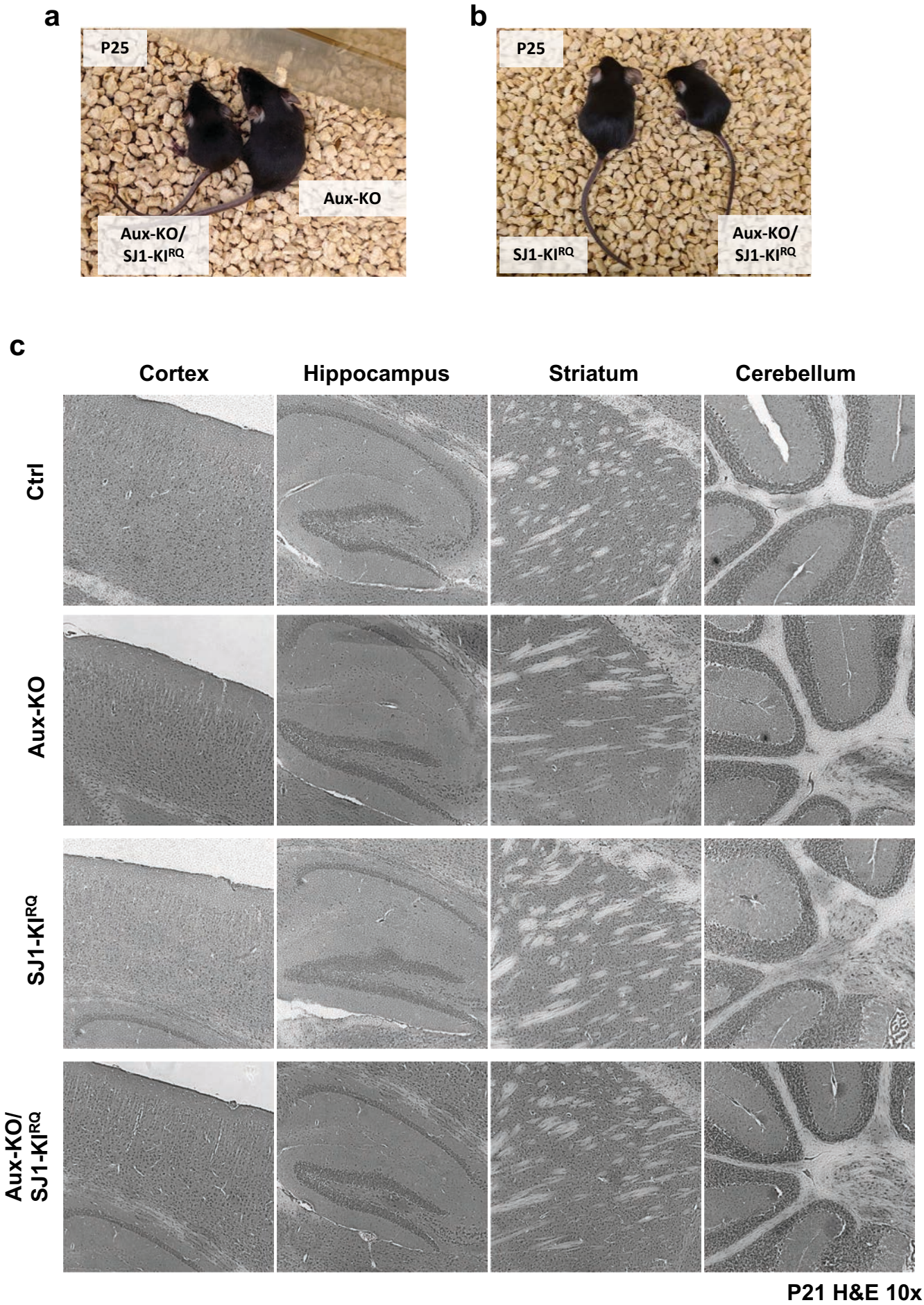


Supplementary Fig 1

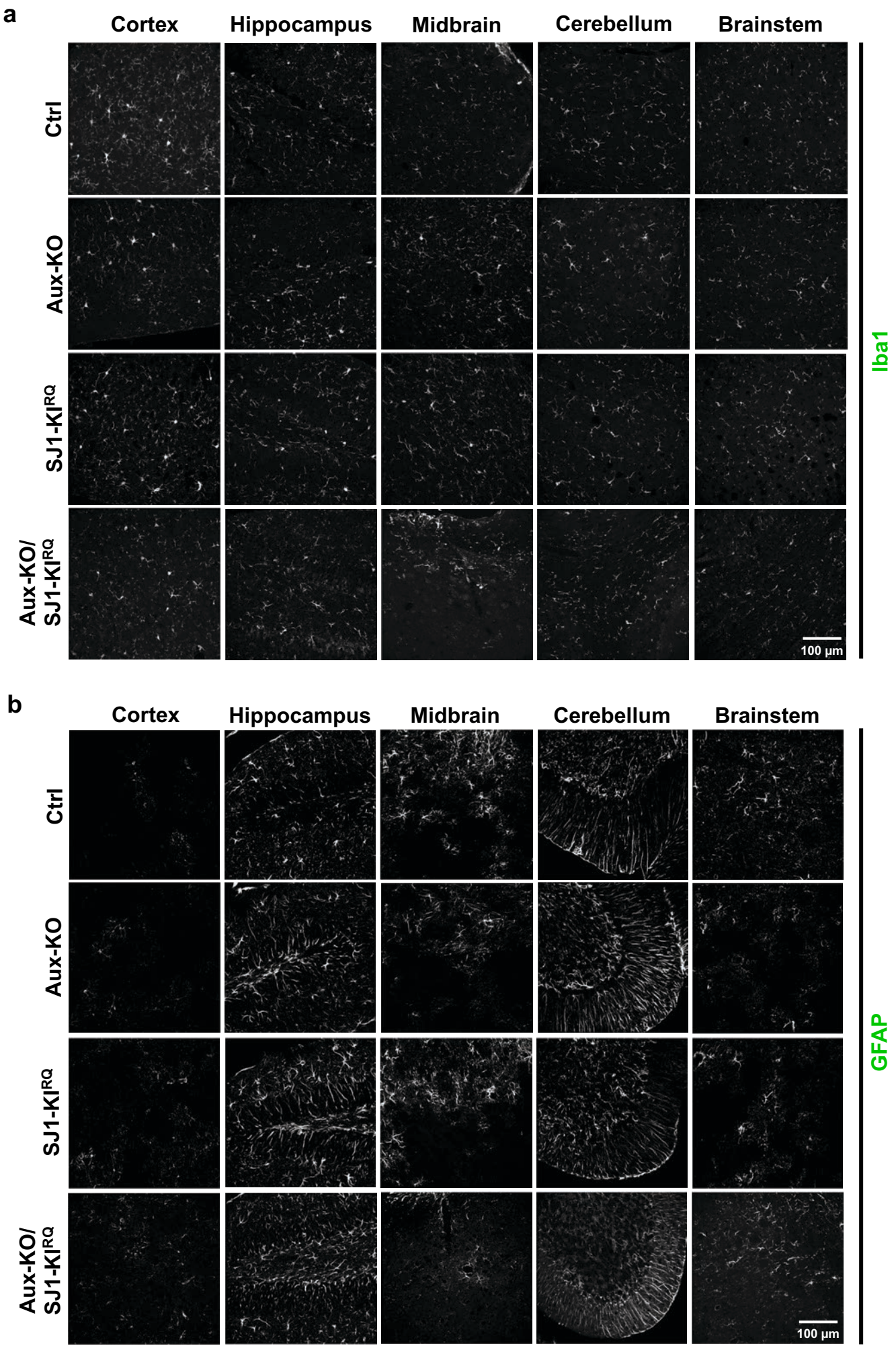


**Supplementary Fig 2**

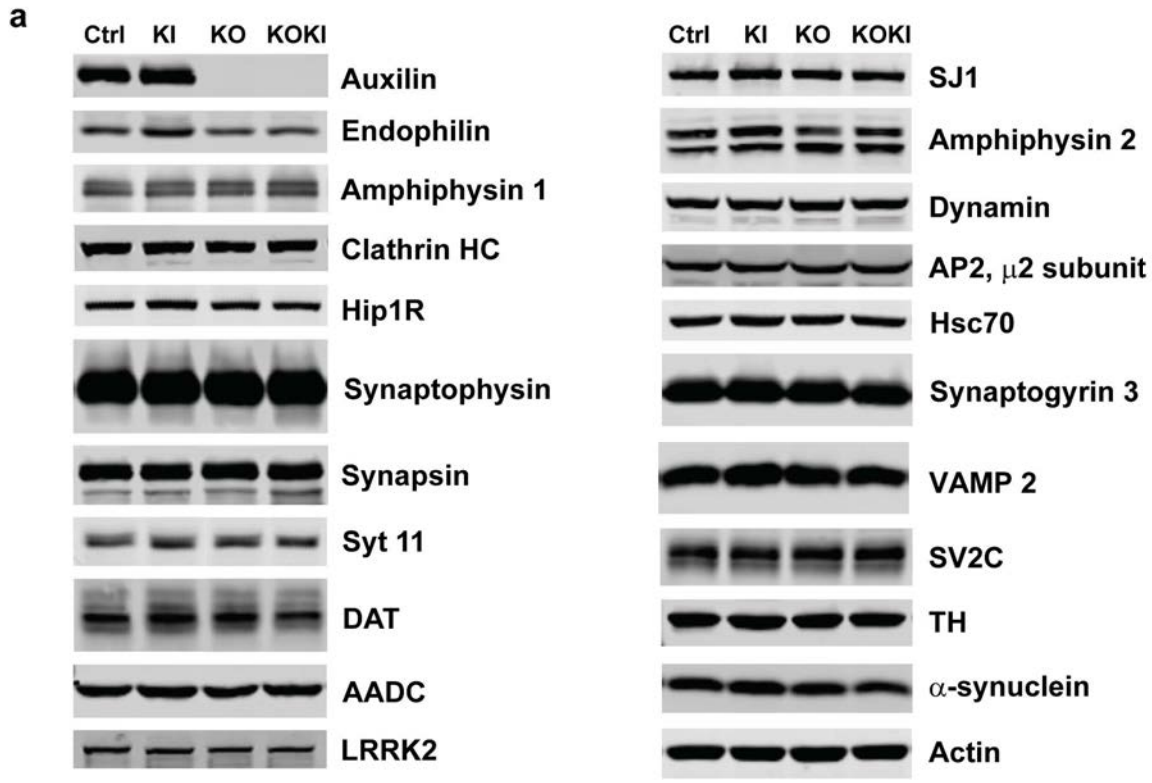


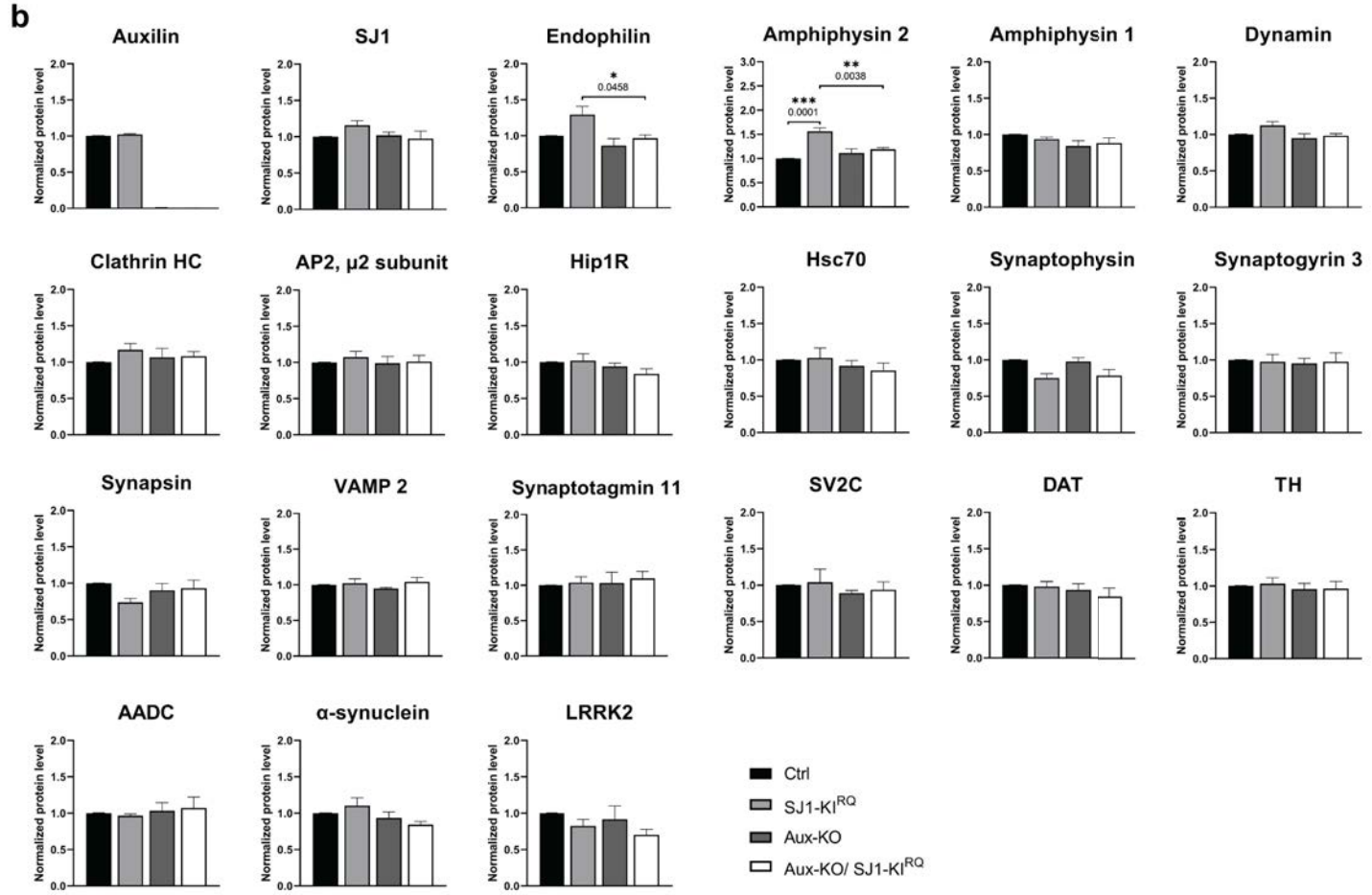


**Supplementary Fig 3**

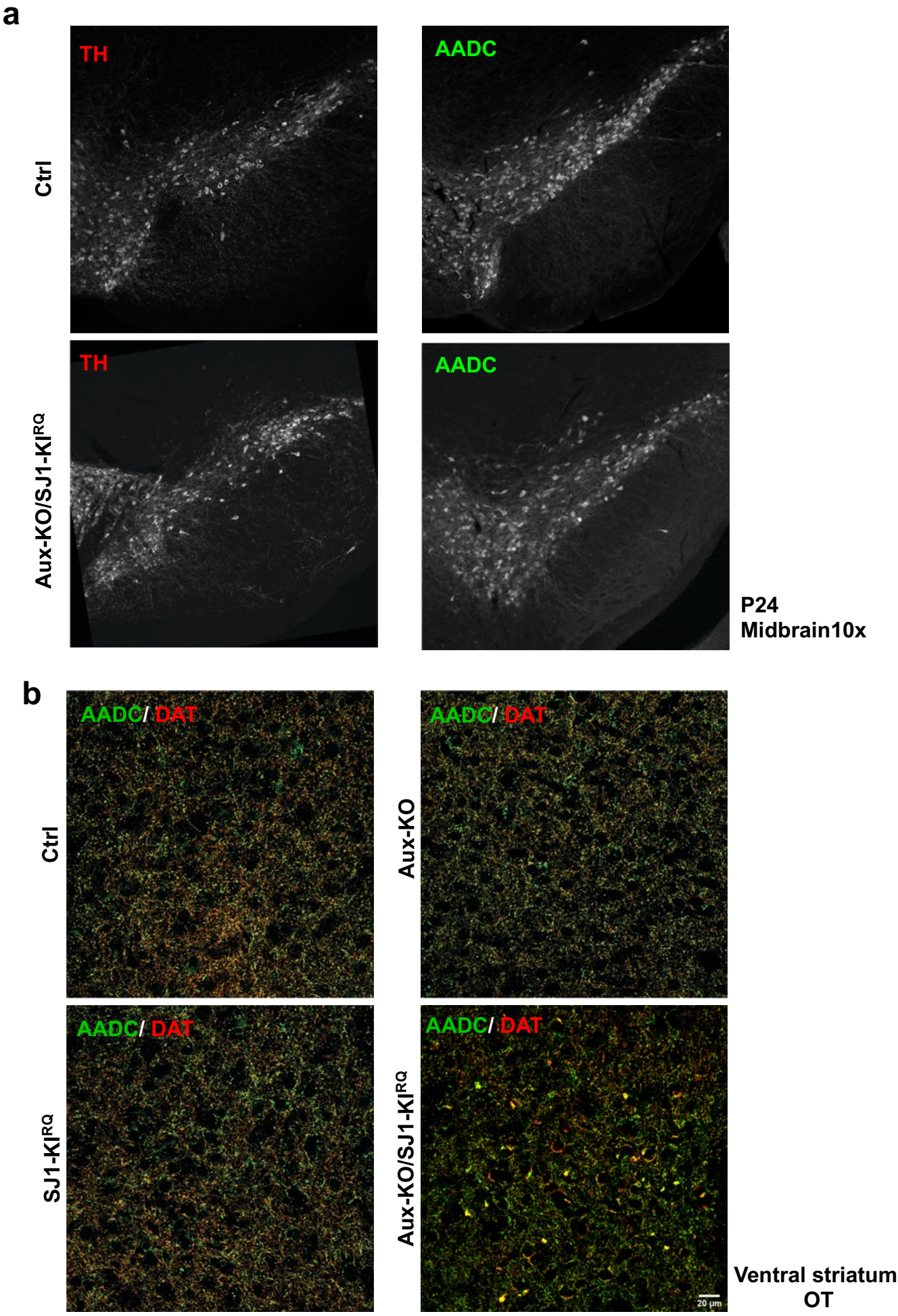


Supplementary Fig 4

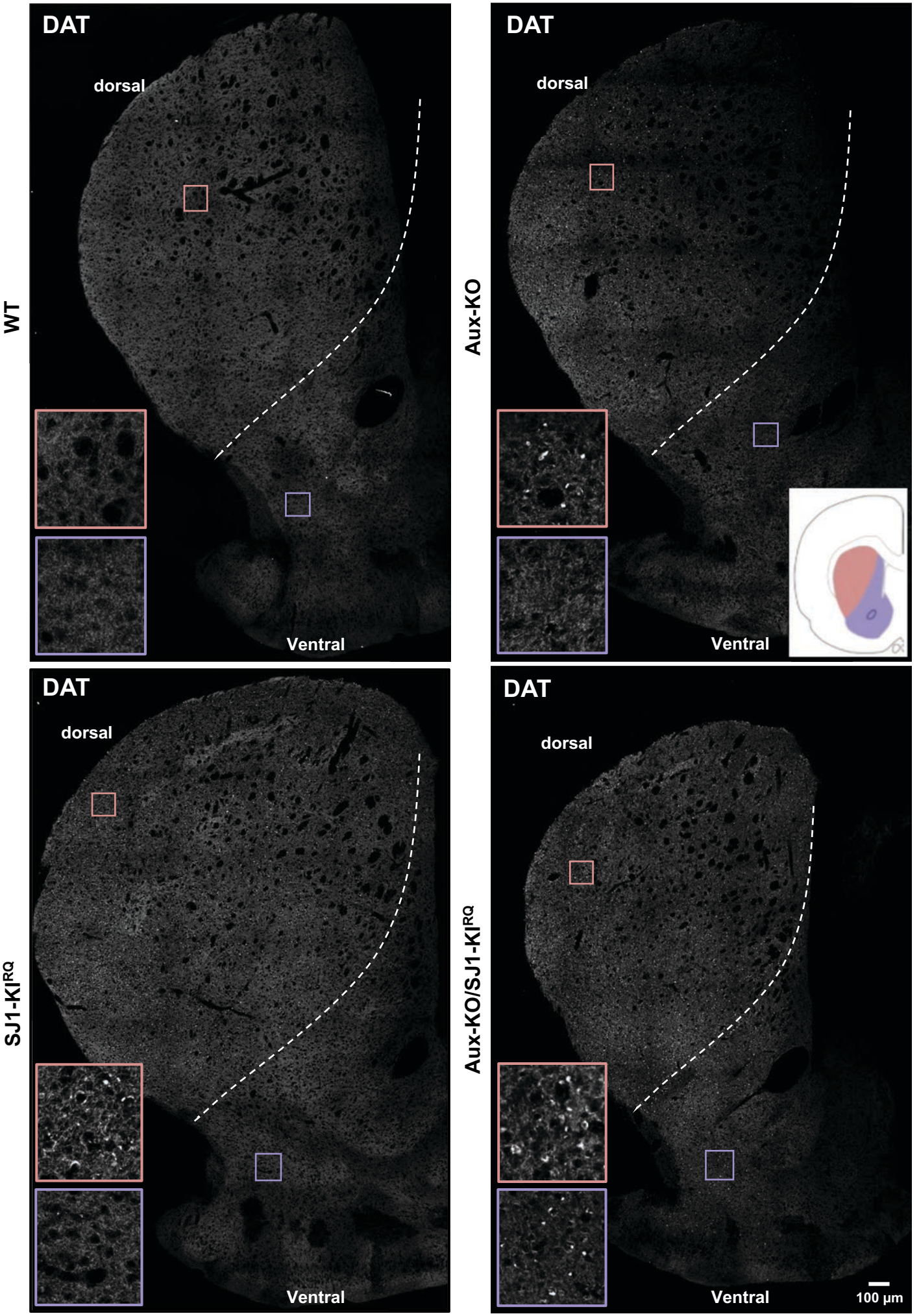


Supplementary Fig 5

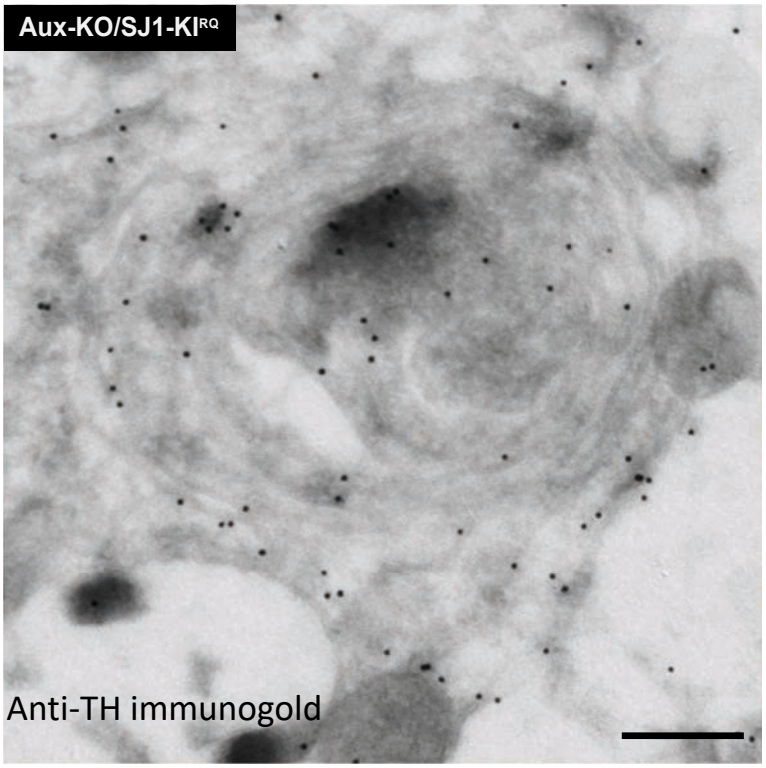


**Supplementary Fig 6**

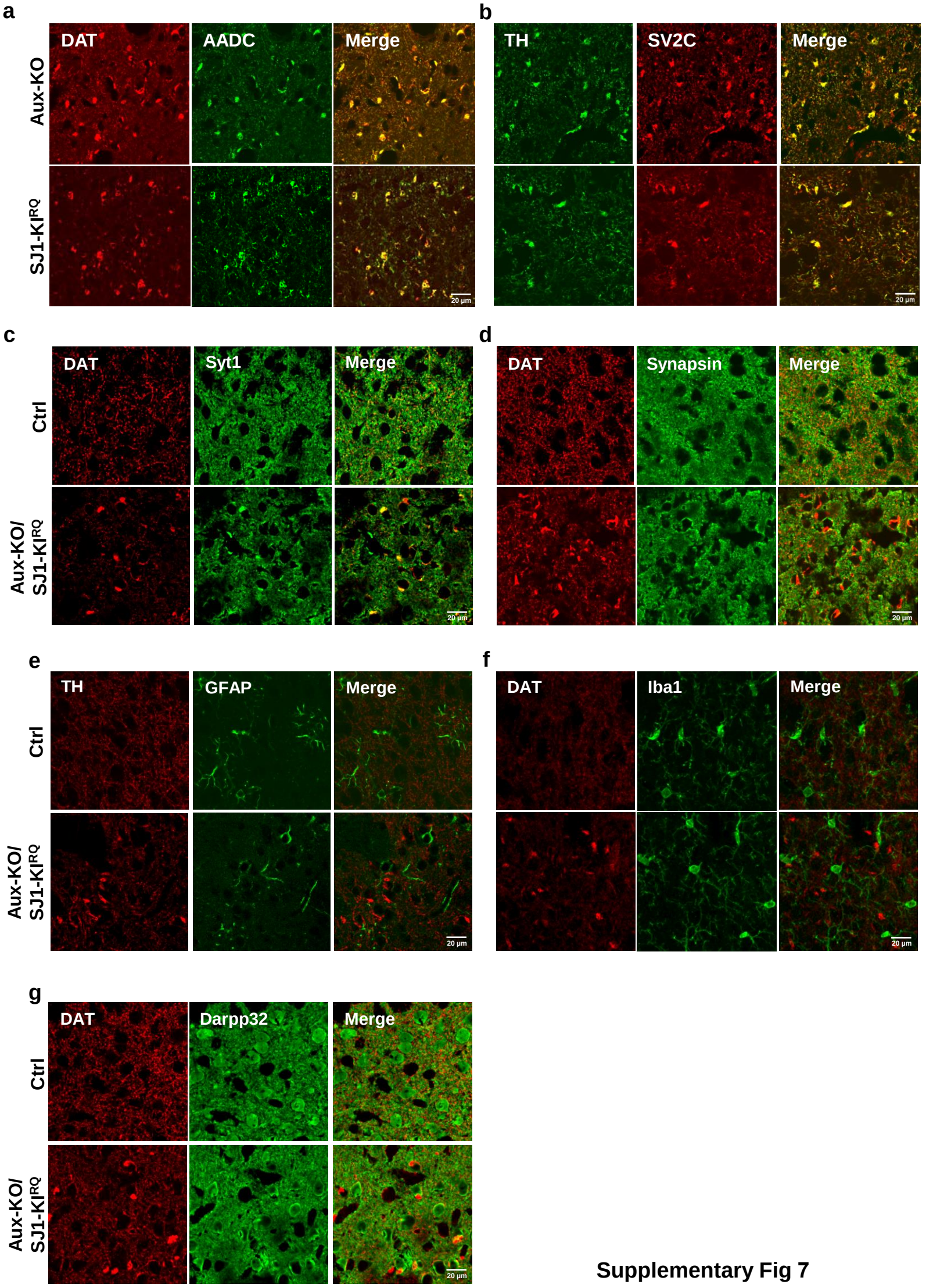


**Supplementary Fig 7**

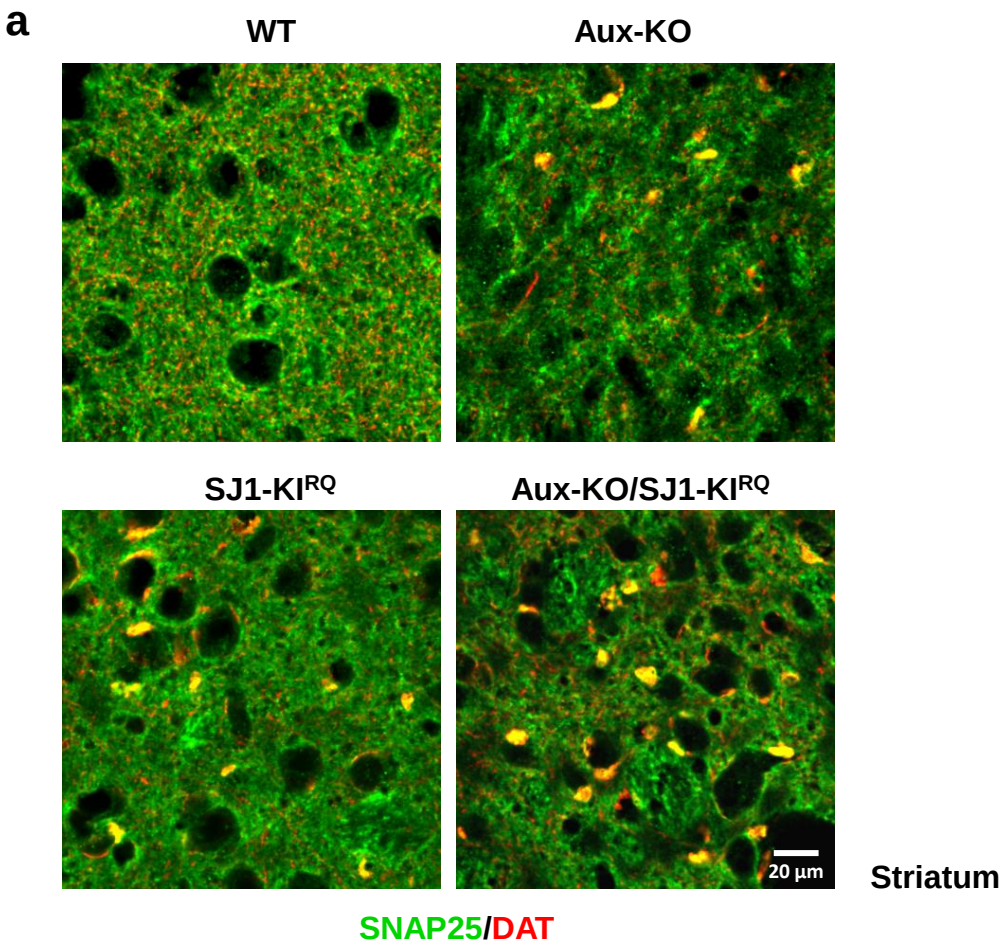


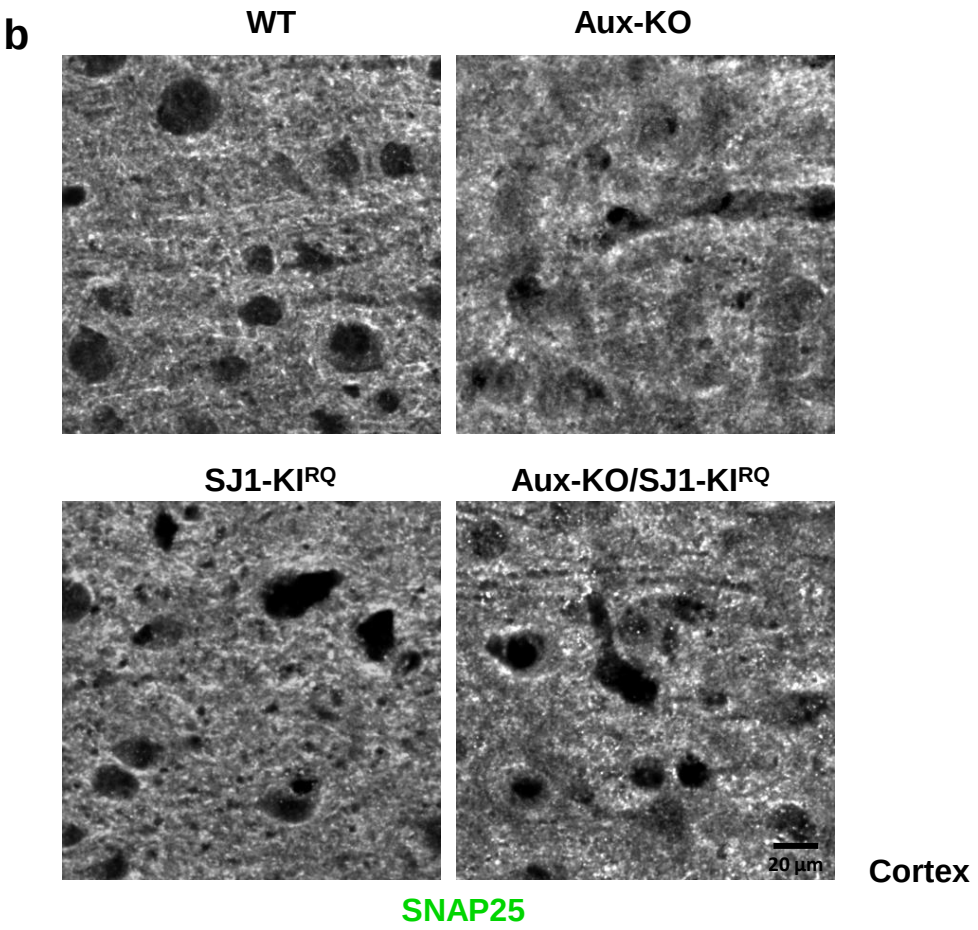


**Supplementary Fig 8**

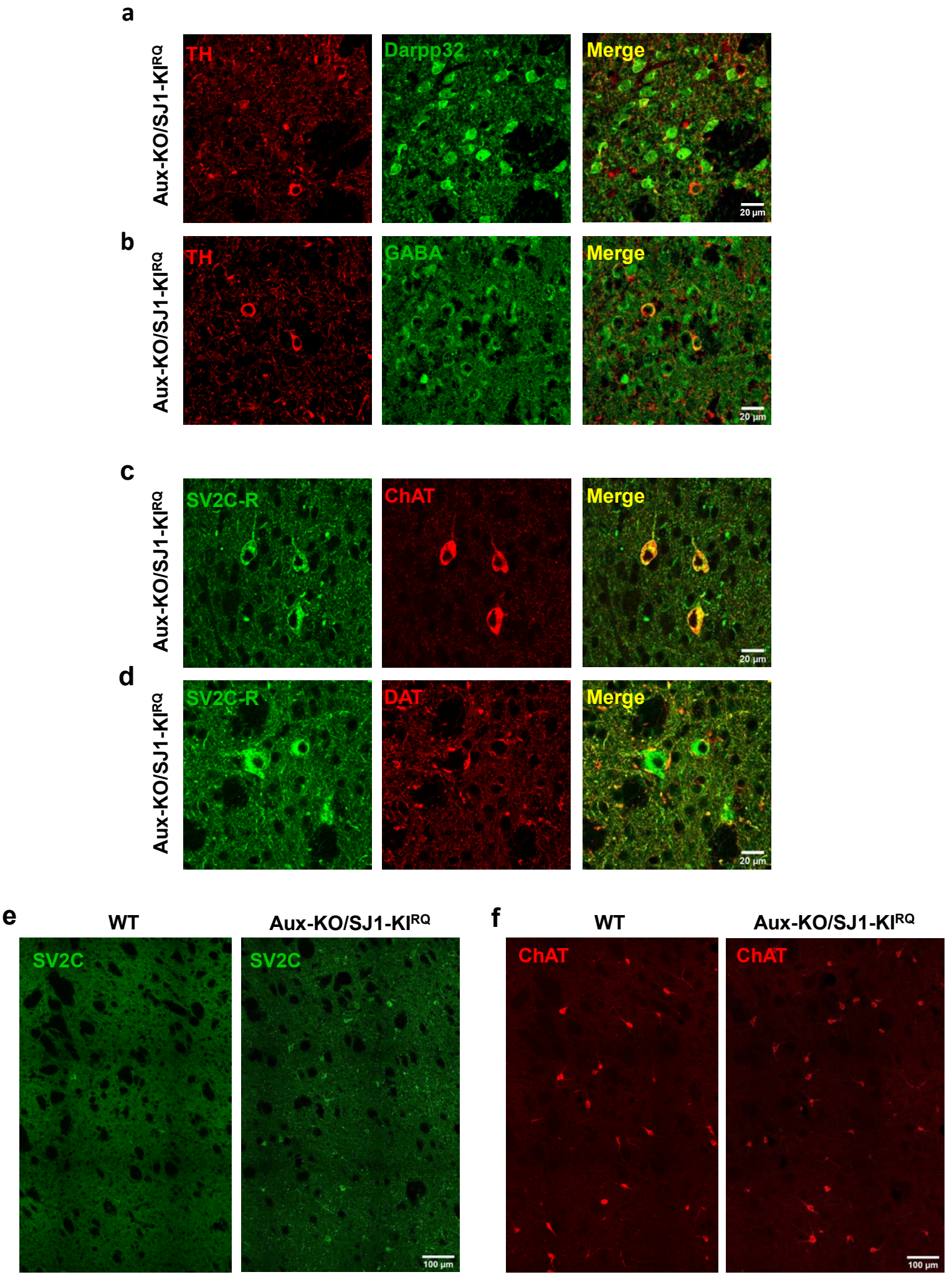


Supplementary Fig 9

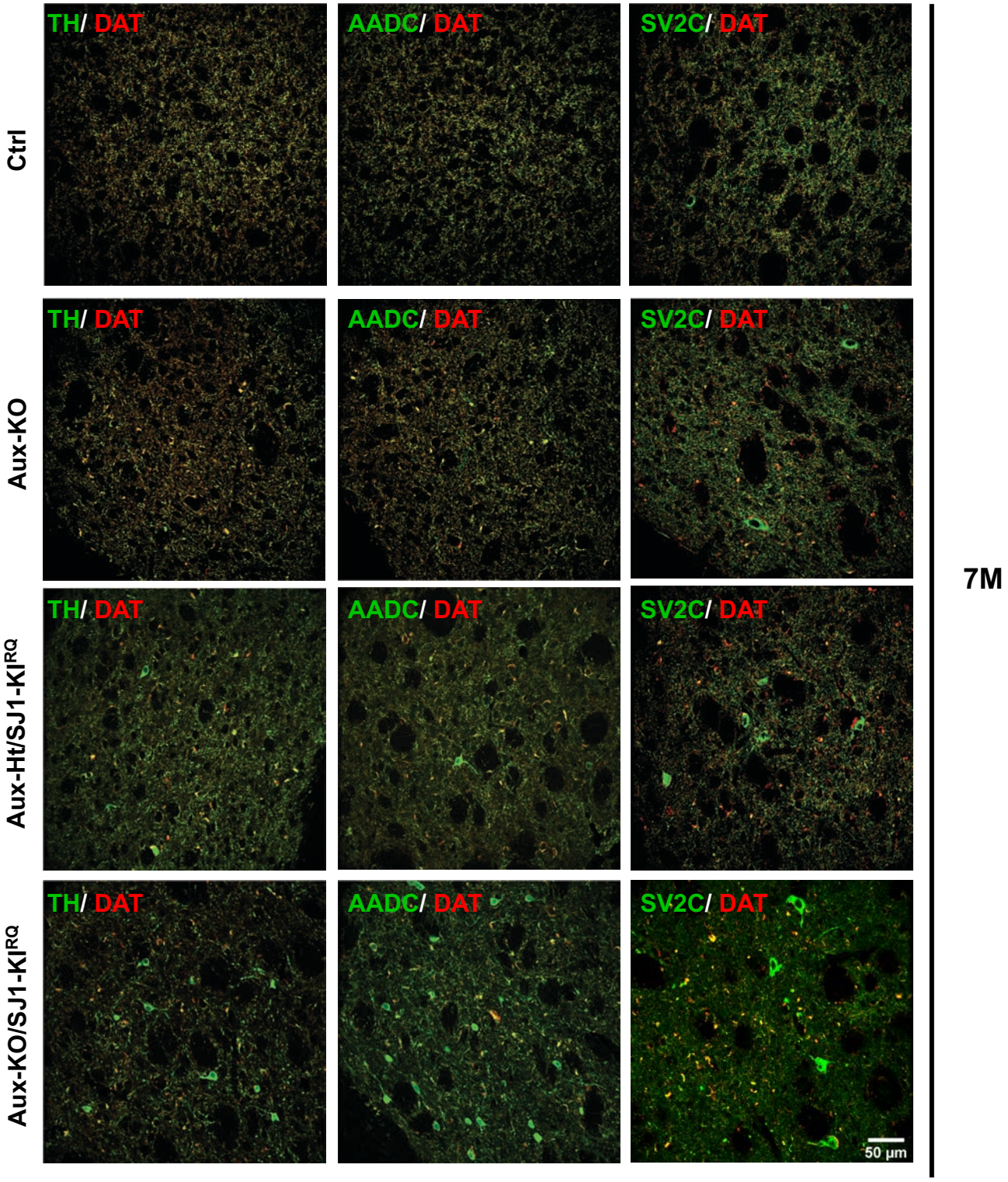


Supplementary Fig 10